
I SPY WITH MY MODEL’S EYE: VISUAL SEARCH AS A BEHAVIOURAL TEST FOR MLLMs

A PREPRINT

John Burden^{*1}, **Jonathan Prunty**¹, **Ben Slater**^{1,2,4}, **Matthieu Tehenan**³,
Greg Davis⁴, and **Lucy Cheke**^{1,4}

¹Leverhulme Centre for the Future of Intelligence, University of Cambridge

²Department of Engineering, University of Cambridge

³Department of Computer Science, University of Cambridge

⁴Department of Psychology, University of Cambridge

ABSTRACT

Multimodal large language models (MLLMs) achieve strong performance on vision-language tasks, yet their visual processing is opaque. Most black-box evaluations measure task accuracy, but reveal little about underlying mechanisms. Drawing on cognitive psychology, we adapt classic *visual search* paradigms—originally developed to study human perception—to test whether MLLMs exhibit the “pop-out” effect, where salient visual features are detected independently of distractor set size. Using controlled experiments targeting colour, size and lighting features, we find that advanced MLLMs exhibit human-like pop-out effects in colour or size-based disjunctive (single feature) search, as well as capacity limits for conjunctive (multiple feature) search. We also find evidence to suggest that MLLMs, like humans, incorporate natural scene priors such as lighting direction into object representations. We reinforce our findings using targeted fine-tuning and mechanistic interpretability analyses. Our work shows how visual search can serve as a cognitively grounded diagnostic tool for evaluating perceptual capabilities in MLLMs.

1 Introduction

Despite their impressive performance, Multimodal Large Language Models (MLLMs) remain opaque in how they internally process and represent visual information. This is partly due to the lack of information disclosed by frontier model developers, and partly due to evaluation approaches: traditional evaluation benchmarks focus on accuracy or alignment with human outputs, but reveal little about the intermediate representations or cognitive-like processes these models may develop or employ. To gain deeper insight, we draw inspiration from investigations in cognitive science, particularly visual search paradigms, which have been used to probe the internal structure of human vision systems. Our goal is to develop a diagnostic toolkit for probing how these models respond to controlled visual challenges. Primarily targeting Marr’s computational level of analysis (Marr, 2000), this approach offers a way to investigate how MLLMs internally represent and prioritise information. We then provide a brief investigation into how these effects are represented in internal activations of MLLMs.

Experimental psychologists seeking to understand the ‘black box’ of the human visual attention system have long used controlled search tasks to probe attentional bottlenecks and feature integration (Treisman and Gelade, 1980; Wolfe, 1994). These reveal regularities and rules underlying visual cognition, while remaining agnostic as to the neural architecture producing them. Here, we take the same experimental approach to interrogate ‘black box’ MLLMs to identify rules governing their visual search behaviour. Our goal is not to optimise model performance, but to uncover regularities and divergences in how these models process visual information—particularly in relation to classic cognitive phenomena like pop-out effects and distractor interference. This approach enables a structured comparison between human and model behaviour, offering insight into the kinds of representations and inductive biases these systems may have developed. Concretely, we present a systematic investigation of visual search behaviour in MLLMs, varying

*Corresponding Author: jjb205@cam.ac.uk

structural components of visual scenes such as the variety of features and the size of distractor sets. In doing so, we provide a targeted investigation of fundamental perceptual capabilities in state-of-the-art MLLMs under zero-shot settings.

2 Background

2.1 Multimodal Large Language Models

MLLMs extend the capabilities of language models by incorporating visual inputs, enabling them to perform tasks such as image captioning, visual question answering, and multimodal reasoning. While earlier vision-language models (VLMs) like CLIP (Radford et al., 2021) and BLIP (Li et al., 2022) focused on learning modality-consistent embeddings for retrieval or generation, MLLMs are typically built by integrating visual encodings into autoregressive language models. Notable examples include Flamingo (Alayrac et al., 2022), which augments a frozen language model with cross-attention to a visual encoder; GPT-4o (OpenAI et al., 2024), which accepts text-image prompts; and LLaVA (Liu et al., 2023), an open-source model that injects visual embeddings into a fine-tuned Vicuna model. These models achieve strong performance across standard image-oriented benchmarks such as VQAv2 (Goyal et al., 2017), OK-VQA (Marino et al., 2019), and MMMU (Yue et al., 2024) often without task-specific tuning. MLLMs differ in how they fuse vision and language, and their internal processing remains largely opaque. Many models are proprietary with limited documentation, and even open architectures offer limited insight into how visual inputs are handled within the model. This means current evaluations overwhelmingly rely on aggregated end-task accuracy, which provides little insight into the internal structure of model reasoning. Given the increasing desire to deploy MLLMs in real-world applications that require strong perceptual capabilities (e.g., medical image analysis (Liu et al., 2025), control of physical robots (Luo et al., 2025)), understanding *how* models achieve these benchmark scores, and in what ways they might fail, is critical. Here, we retain output-based evaluation but reframe it through the lens of controlled experimentation. Just as careful experimentation has provided insight into the internal structures and representations of human cognition, we will use cognitive science inspired visual search paradigms to study MLLM perception.

2.2 Visual Search

Visual search tasks have long been used by psychologists to study human attention and perception. Participants are shown a scene containing a target object and several distractors, and must quickly judge whether the target is present, or identify its location. What makes these tasks powerful is not their difficulty, but their structure—the systematic variation of parameters such as set size, feature complexity, and target presence enables the exposure of latent properties of the underlying cognitive system (Wolfe, 1998, 2020). A classic distinction is between *disjunctive* search, where a target is identifiable from the distractors along a single dimension (e.g., colour—a red square among blue squares, or shape—a square among circles), and *conjunctive* search, where the target can only be identified by a unique combination of features (e.g., colour and shape—a red square among red and blue circles and blue squares). The compositional nature of human visual representations means that disjunctive search typically yields fast, parallel detection—so-called “pop-out” effects—as a pre-attentive feed-forward pass through the early visual system is sufficient to detect the single distinguishing feature (e.g., red among green). However, as conjunctive search requires the attentional binding of two or more primitive features to distinguish the target from distractors (e.g., ‘red’ and ‘square’), reaction times are slower and increase linearly with the number of distractors as each item requires individual inspection.

The distinction between conjunctive and disjunctive search has been shown to be highly reliable across humans and other animals (Orlowski et al., 2015; Reichenthal et al., 2019). Such behavioural phenomena can be used to understand the nature of the processes the visual system is performing when allocating attention and to predict behaviour in novel scenarios (for example, one can predict that a human will quickly identify and locate a coffee stain on a white carpet, but not on a colourful patterned rug). Using careful manipulation of inputs and observing changes in behaviour, the underlying structure of informational processes can be inferred. This makes visual search tasks particularly suitable for interrogating black-box models like MLLMs where the internal representations may be opaque. Structured behavioural experiments can reveal the presence, predictability and human-likeness of search strategies. Understanding visual search in humans has real-world value, for example for selecting the safest display layouts in cars (Smith et al., 2015). Similarly, understanding visual search in MLLMs may be valuable for determining how to best present tasks to multimodal systems to maximise the likelihood of success. For example, road signs are designed to be salient to human drivers, but it’s becoming increasingly important to identify whether the same features would be salient to self-driving cars.

3 Visual Search Experiments

We adapted three visual search experiments for MLLMs: **Circle Sizes**, **2 Among 5** and **Light Priors**. Each targets a specific visual feature known to induce the “pop-out” effect in humans: size (Samiei and Clark, 2022), colour (Wolfe et al., 2010; Wolfe and Horowitz, 2004) and light source direction (Adams, 2007), respectively. Each experiment is described in detail in Sections 3.1–3.3. We include two target localisation variants evaluating levels of precision:

- **Cells:** The image is divided into a 2×2 grid, and the model must identify the grid cell containing the target (always present). Accuracy is the proportion of trials in which the correct cell is identified.
- **Coordinates:** The model must return the coordinates of the target. Performance is evaluated using Euclidean distance from the chosen point to the centre of the target.

We evaluate a selection of MLLMs, comprising both closed source and open source models. Specifically, we evaluate GPT-4o (OpenAI et al., 2024), Claude Sonnet 3.5 (Anthropic, 2024), Llama 3.2 90B (Meta AI, 2024). Full details of the model are provided in Appendix C. A selection of other models are also evaluated in Appendix B. We also compare against a human baseline ($N = 90$). Humans are generally highly accurate in visual search tasks, and processing differences between experimental conditions are usually identified using response times. However, by limiting stimulus presentation time (e.g., to 1500ms) we can compare humans and LLMs using accuracy scores alone. Further details of the human portion of the experiment are provided in Appendix I. All the code needed to replicate our experiments is provided on [Github](#).

3.1 Experiment 1: Circle Sizes

Our first experiment was designed to investigate whether MLLMs, like humans, show ‘pop-out’ effects in disjunctive search tasks – that is, tasks in which the target can be easily distinguished from distractors by a single change in a simple visual feature. Object size is one such feature that can be detected pre-attentively in human subjects (Proulx, 2010). Figure 1 illustrates how we systematically manipulated the radius of a target circle amongst matched distractors using three experimental conditions: Small (22.5 pixels), Medium (25 pixels) and Large (30 pixels). The number of distractors varied from 0 to 49 across trials, and all circles were randomly placed on a white 400×400 pixel background and rendered without overlap. Target and distractor circles were presented in the same colour, which was randomly sampled from red, green and blue. If MLLMs process size as a visual primitive, we would expect them to locate the target circle in the Large condition with high accuracy and precision, irrespective of distractor numbers. We would also expect that this ‘pop-out’ effect would be attenuated when size differences are less salient in Small and Medium conditions.

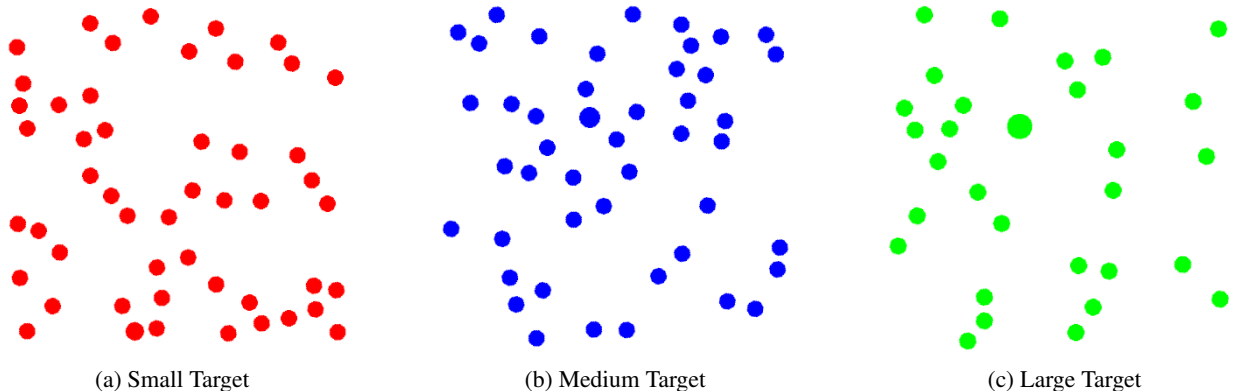


Figure 1: Circle Sizes task. Examples from the three experimental conditions. The target is always the single circle that is larger than the rest. The colour of all circles is always the same and is sampled from red, blue and green.

Figure 2 presents model performance on the Circle Sizes task in the cells variant. GPT-4o exhibits a clear pop-out effect: its accuracy for Large targets is high ($M = 83\%$) and remains stable across increasing numbers of distractors ($r = -0.028$, $p = 0.082$). Accuracy for Medium targets also remains high ($M = 72\%$), though it shows a modest decline with set size ($r = -0.102$, $p < .001$). In contrast, performance for Small targets ($M = 43\%$) is lower, and declines more markedly as distractor count increases ($r = -0.177$, $p < .001$). Notably, GPT-4o’s response pattern closely mirrors that of human participants, who showed pop-out in the Large condition, near pop-out in the Medium condition, but declining accuracy for higher distractor numbers in the Small condition (see Appendix I). Claude Sonnet also demonstrates sensitivity to target size, with performance systematically decreasing across conditions. However, unlike GPT-4o, it

does not exhibit set size independence in any condition ($r_s < -0.110$, $p_s < .001$). LLaMA 90B fails to differentiate between target size conditions, exhibiting poor accuracy scores throughout (though is marginally better on the Large targets). The difference between models is particularly evident in the coordinates task variant (see Appendix Figure 8). GPT-4o localises Medium and Large targets with minimal error; Claude Sonnet maintains low error rates only for Large targets; whereas Llama 90B exhibits high error rates across all three conditions, with unexpectedly high error for Large targets due to a high number of invalid coordinate responses (see Appendix D). These findings suggest that more capable models, particularly GPT-4o, exhibit robust and human-like size-driven salience effects in disjunctive search. More detailed human results and set-size correlation analyses are reported in Appendix I and F.

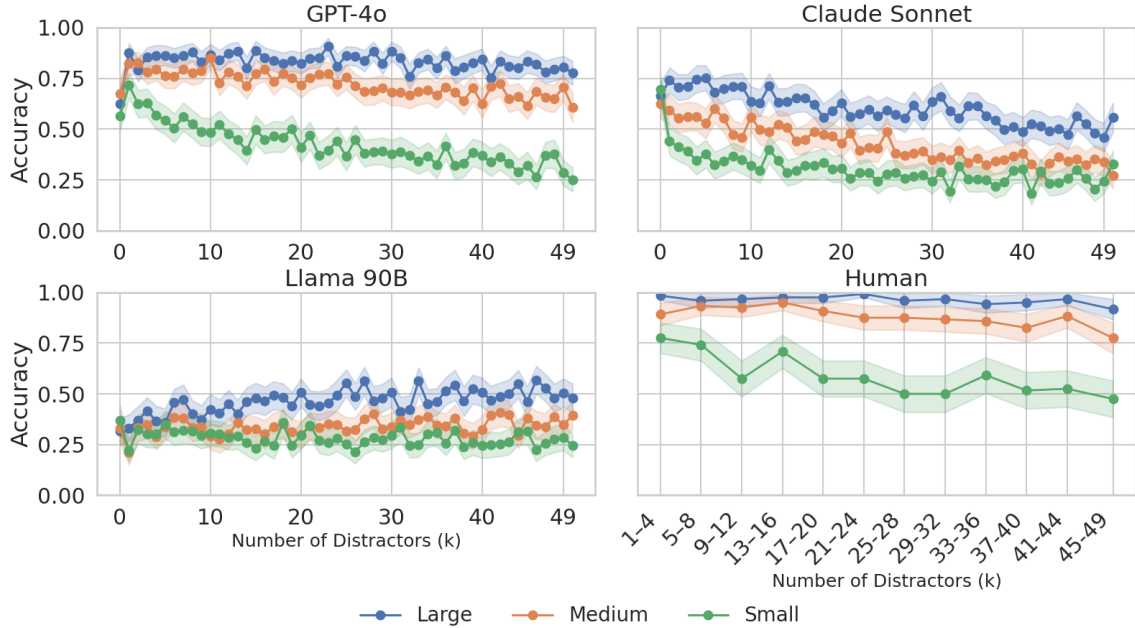


Figure 2: Results for Circle Sizes on Cells.

3.2 Experiment 2: 2 Among 5

In Experiment 1, we demonstrated that MLLMs show a pop-out-like pattern of behaviour in disjunctive search. In Experiment 2, we investigated whether MLLMs demonstrated human-like attentional limitations for *conjunctive* search by adapting the “2 Among 5” task from Wolfe et al. (2010) – the goal of which is to locate a target “2” among distractor “5”s (or *vice versa*). These digits are mirror images of each other, and are more complex than simple shapes (e.g., circles) as they consist of a combination of five line segments. We manipulated search type across three experimental conditions (see Figure 3): Disjunctive, Shape Conjunctive and Shape-colour Conjunctive. In the Disjunctive condition, target digits differ in colour from all other distractors, enabling parallel detection based on colour alone. In the Shape Conjunctive condition, however, all digits are the same colour, requiring the representation of both spatial configuration (i.e., the combination of line segments) and chirality (i.e., a “5” or “2”) to identify the target. Finally, in the Shape-Colour Conjunction condition, the target must be differentiated by a unique combination of both colour and spatial features (e.g., a “red 2”) amongst distractors that have other shape-colour combinations (e.g., “red 5”, “blue 2” etc.). In humans, ‘binding’ primitive visual features to form more complex object representations requires attentional resources (Treisman and Gelade, 1980), resulting in serial search behaviour as potential targets require individual inspection, leading to search times that increase linearly with distractor numbers. If MLLMs have similar representational limits, they should show poorer performance in Shape Conjunctive and Shape-Colour Conjunctive conditions relative to the Disjunctive condition.

As in the previous experiment, targets and distractors were randomly placed on a 400×400 white background, but were also assigned a random rotation between 0 and 360 degrees. As before, digit colour was randomly sampled from red, green and blue, though for Disjunctive and Shape-Colour Conjunctive conditions two colours were sampled without replacement and assigned appropriately to target and distractors. The number of distractors present in each trial was also

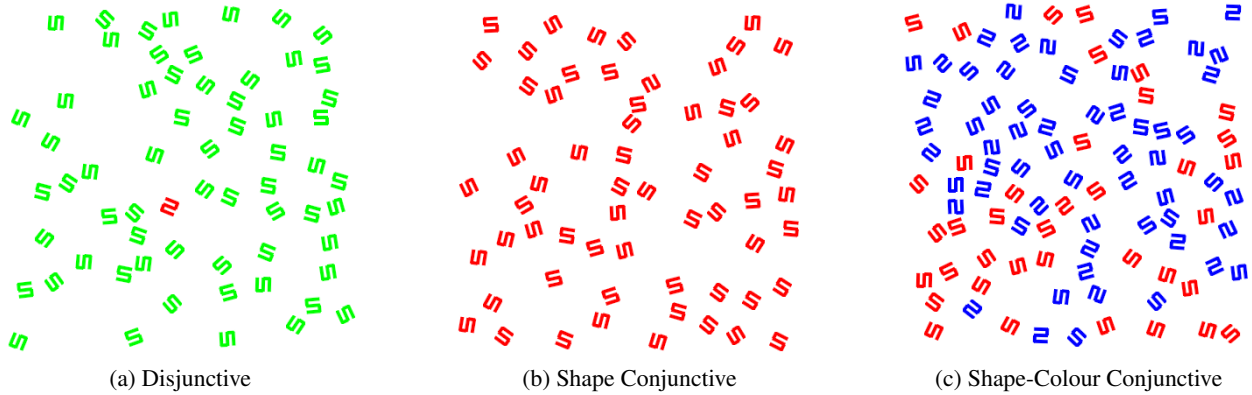


Figure 3: Example stimuli from the 2 Among 5 task, illustrating the three experimental conditions. pronounced In all examples, the target “2” is coloured red. (a) **Disjunctive**: The target differs from distractors by colour. (b) **Shape Conjunctive**: All digits share the same colour, requiring shape discrimination. (c) **Shape-Colour Conjunctive**: The target is uniquely defined by both shape and colour, with distractors sharing at most one feature. Target and distractor colours are randomized across trials.

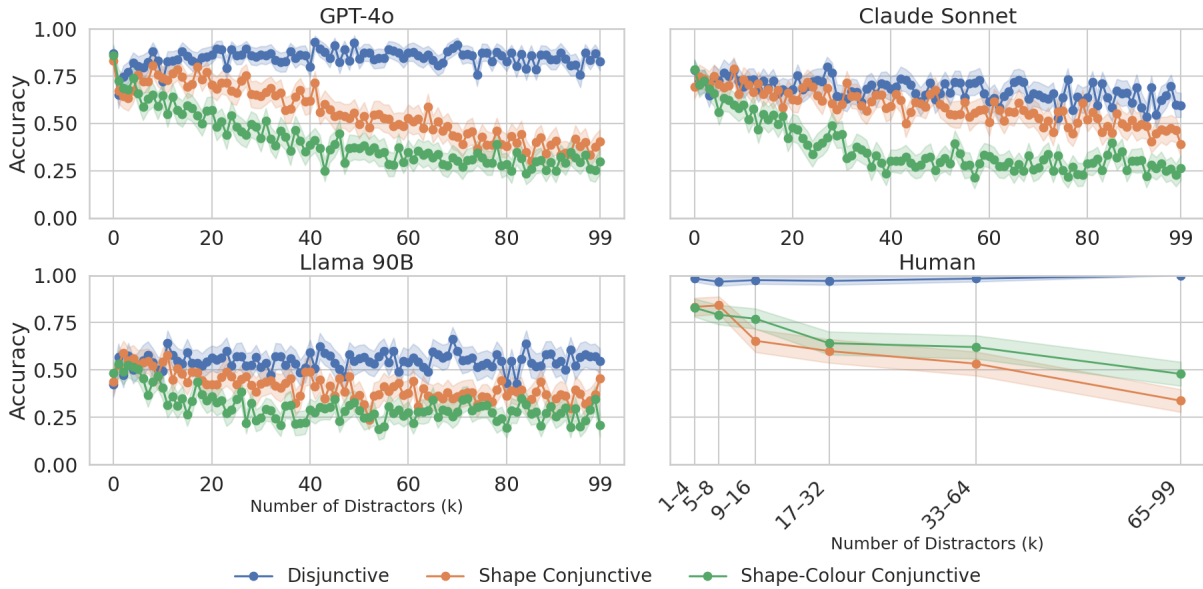


Figure 4: Results for the 2Among5 task — Cells mode. The shaded region denotes the 95% confidence interval.

varied from 0 to 99. We tested both “2 among 5” and “5 among 2” cases, in order to control for potential asymmetries or biases in the model’s representations.

Figure 4 shows model performance for “2 Among 5” and “5 Among 2” tasks combined in the cells variant. GPT-4o showed high performance in the Disjunctive condition ($M = 85\%$) which was also flat across set sizes ($r = 0.017$, $p = 0.249$), replicating the pop-out effects that we found in Experiment 1 and in our human experiments. GPT-4o also showed human-like limits for conjunctive search, as its performance in Shape Conjunctive ($r = -0.267$, $p < .001$) and Shape-Colour Conjunctive ($r = -0.244$, $p < .001$) conditions declined as the number of distractors increased. Claude Sonnet showed a slight decline in accuracy with increasing set size in the Disjunctive condition ($r = -0.065$, $p < .001$), but was strongest in this condition overall ($M = 68\%$). However, it showed a much smaller performance gap between Disjunctive and Shape Conjunctive, which may be suggestive of representational differences between the models. Although Llama 90B’s performance was generally poor, it did show an advantage in the Disjunctive condition ($M = 55\%$), perhaps suggesting a crude salience heuristic. This pattern was corroborated in the coordinate-based

localisation task (Appendix Figure 9), where error rates for GPT-4o and Claude Sonnet show clear differences between the conditions reflecting highly precise disjunctive search, but increasing error-rates with set-size for conjunctive search. Llama 90B, however, did not distinguish between search tasks, with high error in all three conditions.

3.3 Experiment 3: Light Priors

Thus far, we have demonstrated that some MLLMs, like humans, show set-size *independent* detection of targets when they can be distinguished by a single primitive visual feature (i.e., disjunctive search), but show set-size *dependent* search performance when representational binding of multiple features is required (i.e., conjunctive search). In a third experiment, we investigated whether MLLMs possess more sophisticated representations that incorporate assumptions about how objects appear in the real world. Classic work in cognitive science has found that humans have a ‘light-comes-from-above’ prior due to their experience of the natural world (Enns and Rensink, 1990). This is incorporated into low-level visual perception such that objects lit from the top or bottom can be rapidly detected – and bottom-lit objects, due to their novelty, are particularly salient (Enns and Rensink, 1990).

To test whether MLLMs also incorporate natural scene priors in visual search, we adapt a visual search task from cognitive science (Adams, 2007). In this task, each image contains a number of shaded circles designed to resemble 3D spheres illuminated from a specific direction. The goal is to identify the sphere that is the ‘odd one out’, that is lit from the opposite (180°) direction to distractors, but is otherwise identical. Here, we defined four task variants: Top, Bottom, Left, and Right, corresponding to the direction the target appeared to be lit from. Distractor numbers varied between 0 and 17 per trial. The spheres were rendered in greyscale to avoid introducing colour cues, and were randomly placed at least 20 pixels apart in a medium-toned greyscale circle within the image without overlap. We also included a black border to ensure a consistent maximum distance of spheres from the image centre. Example stimuli are shown in Figure 5.

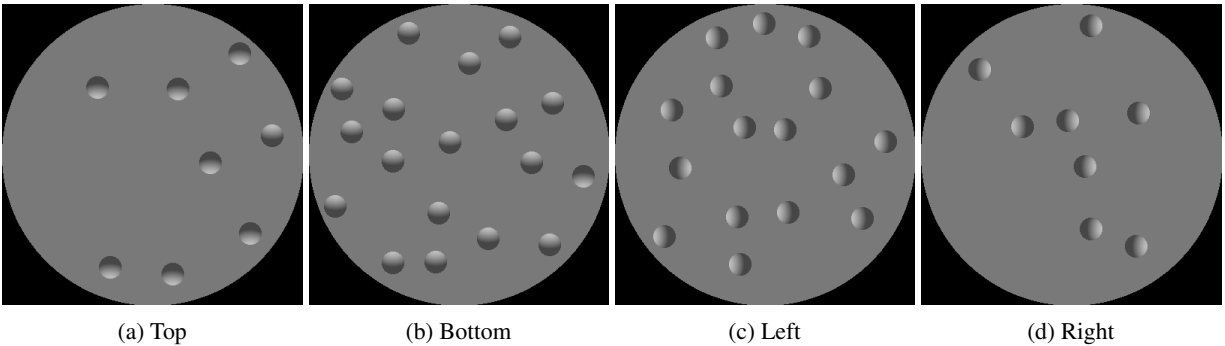


Figure 5: Light Priors Task: Circles are shaded with directional gradients, mimicking the shading on a sphere if lit from different directions. The subject must identify the target lit from a specific direction.

Figure 6 illustrates the results for the Light Priors cells task. Although we don’t see a pattern indicative of pop-out—as models show overall reduced accuracy and flat performance across set-sizes in *all* conditions—we do see clear differences between light-source conditions. For two or more distractors, as at least two distractors are required for an accurate “odd-one-out” decision, the pattern of results from GPT-4o shows remarkable similarity to our human baseline, with performance advantages for vertical (top and bottom-lit) relative to horizontal gradients (left and right-lit). Interestingly, we also see a clear performance advantage for bottom-lit ($M = 73\%$) relative to top-lit ($M = 55\%$) spheres, matching human behaviour. Claude and Llama’s performance on this task was poorer overall (GPT-4o: $M = 52\%$, Claude: $M = 34\%$, Llama: $M = 46\%$), but both showed a vertical-gradient advantage, and Claude (though not Llama) showed the highest accuracy for bottom-lit spheres. In the coordinates task, GPT-4o error rates (Appendix Figure 10) mirror the cell variant almost exactly, Claude Sonnet shows a clear performance advantage for bottom-lit spheres relative to the other lighting directions, whilst Llama 90B demonstrates slightly better performance for vertical-gradient spheres.

4 Fine-tuning

Our experimental results have demonstrated that MLLMs, like humans, show capacity limits in conjunctive search. Human performance on conjunctive search tasks has been shown to improve after training (Czerwinski et al., 1992). Similarly, we tested whether MLLM performance on conjunctive tasks could be improved through fine-tuning. *Supervised Fine-tuning* (SFT) refers to an additional task-specific training step used to improve the performance of a

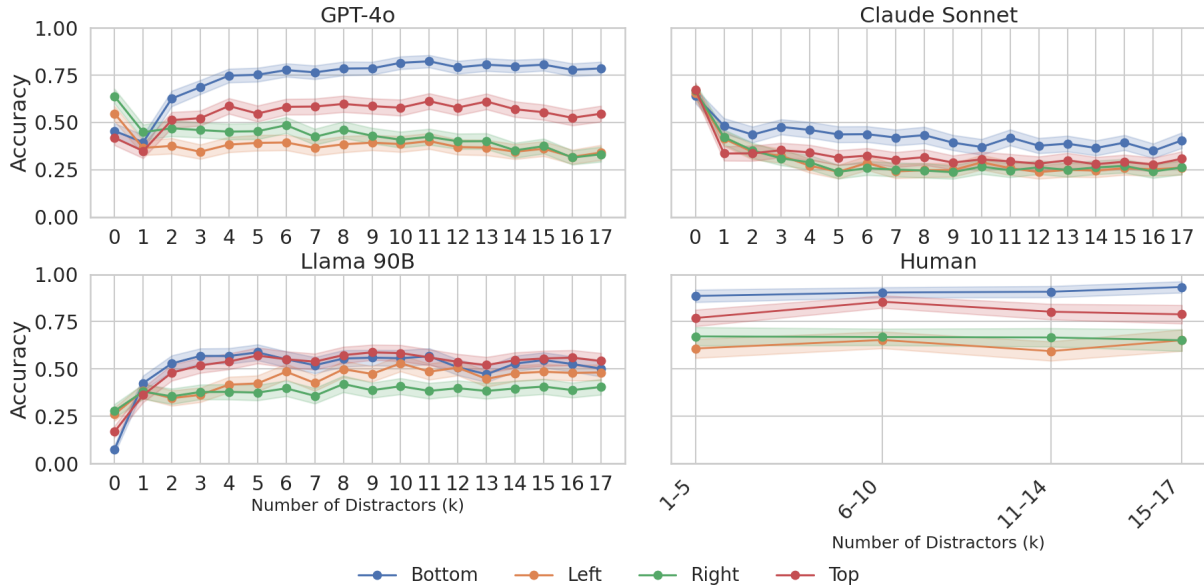


Figure 6: Results for the Light Priors task — Cells mode (three models + human baseline).

language model in a particular domain. Here, we fine-tuned GPT-4o on examples from the Shape Conjunctive variant of the 2 Among 5 task, paired with ground-truth cell responses. We trained models with datasets generated with a different seed, with sizes 10 and 100 for three epochs, and 1000 for a single epoch.² The training data included only items with 0–49 distractors; test data included the full range up to 99, allowing us to assess generalisation beyond the training distribution.

Figure 7 shows accuracy on the Shape Conjunctive 2 Among 5 task under the *Cells* evaluation. Even minimal fine-tuning (10 examples) yields modest gains, while 100 and 1000 examples produce substantial improvements, though not to the level of pop-out. Notably, these gains extend to out-of-distribution set sizes (50–99 distractors), indicating fine-tuning can provide more generalisable visual search strategies. We probed this further by evaluating transfer to related tasks: Shape-Colour Conjunctive 2 Among 5 and Shape Conjunctive “T among L” (details in Appendix H). As shown in Figure 7, performance improves on the “T among L” task, especially at higher distractor counts, suggesting that the model transfers its search behaviour across shape domains³. No such improvement occurred for Shape-Colour Conjunctive 2 Among 5, indicating transfer is strongest when both training and evaluation conditions target similar feature domains (e.g., shape), and weakest when the downstream task requires integration of additional non-trained feature cues (e.g., shape and colour). The full set of results are plotted in Appendix H.

5 Mechanistic Interpretability

While behavioural methods can provide valuable information about cognition, these insights can also be informed by cognitive neuroscience — which investigates how such processes are grounded in the structure and function of the human brain (Marr, 2000). In a similar spirit, we used methods from mechanistic interpretability (Lin et al., 2025) to investigate the internal structures of MLLM representations. Considering results found for simple features (e.g., colour) in CNNs and transformer models (Raghu et al., 2021; Caron et al., 2021; Zeiler and Fergus, 2014), we hypothesised that disjunctive search tasks, which depend on primitive visual features, would engage earlier layers of the network, whereas more complex conjunctive search tasks requiring feature binding would recruit deeper layers. Here, we focus our analysis on Llama 90B, the largest open-weight model we tested, and present findings from the 2 Among 5 task, in which it showed the most reliable search performance.⁴ Appendix Figure 20 shows the results for linear and

²The 1000-example model was also trained for three epochs, but after the first epoch we observed a collapse in behaviour, with nonsensical outputs. We report only the model after one epoch.

³Note that these results are binned by number of distractor for clarity. The corresponding unbinned plot is presented in Appendix H

⁴Full mechanistic interpretability analyses, including results from all three experiments, can be found in Appendix K

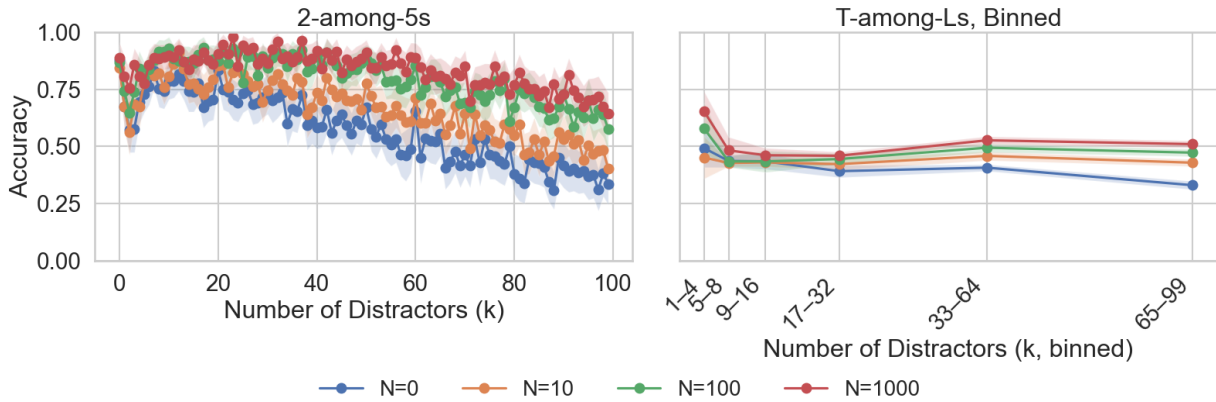


Figure 7: Evaluation of GPT-4o fine-tuned at various dataset sizes for the 2 Among 5 Shape Conjunctive task (left) and the T-among-Ls Shape Conjunctive task (right)

non-linear probes trained to identify the most relevant network features for performing the task. This analysis showed that Disjunctive search tasks were resolved at earlier layers relative to conjunctive tasks, and despite similar behavioural performance, probes were able to distinguish between the two conjunctive search tasks, with Shape-Colour Conjunctive recruiting much deeper network layers than Shape Conjunctive.

6 Related Work

We have presented a thorough, systematic investigation of visual-attentional search capabilities in MLLMs, including three distinct search tasks, fine-tuning and mechanistic interpretability experiments, and comparisons to human baselines. Our findings align with those of Campbell et al. (2024), who included a brief visual search task within a broader set of experiments exploring human-like capacity limits in MLLMs. They reported serial-search-like behaviour in a conjunctive search task and argued that such limitations reflect compositional representations (e.g., “blue circle” represented as “blue” and “circle”, not “BlueCircle”), though their analysis was limited to a single feature and did not provide a matched comparison between disjunctive to conjunctive search tasks. They speculate that improvements on conjunctive search tasks may require introducing a serial search mechanism, or an equivalent process for decomposing images into manageable parts, if compositionality was to also be preserved. We found that fine-tuning on a conjunctive search task (2 Among 5) improved performance, though not to the level of pop-out, and did so even for larger set sizes absent from the training data. Analogous training effects have also been found in human studies, where consistent practice over many sessions can lead to those specific compositional representations becoming “unitized” (i.e., perceived more holistically), attenuating the binding problem (Czerwinski et al., 1992). Unlike human participants, who typically exhibit only partial transfer effects (Su et al., 2014; Ding et al., 2023), GPT-4o showed mild transfer to a distinct conjunctive search task (T-among-L), suggesting that fine-tuning may enhance MLLM performance through a different mechanism. Other work has also tried to improve the visual capabilities of MLLMs by augmenting them with specialized mechanisms. V* (Wu and Xie, 2023) incorporates contextual knowledge to guide attention, while the Target and Context-Aware Transformer (Ding et al., 2022) fuses object- and scene-level features for efficient zero-shot visual search. ViSioNS (Travi et al., 2022) introduces scanpath modelling to align image processing with human attentional patterns.

More broadly, visual search can be situated within the field of visual question answering (VQA), where models are evaluated on their ability to reason about visual scenes. MLLMs have been widely applied to this setting, often with architecture-specific optimizations or fine-tuning strategies. For comprehensive overviews of VQA and its extension to multimodal foundation models, we refer the reader to recent surveys (Wu et al., 2017; Kuang et al., 2025). In contrast to most work in this area, our goal is not to improve model performance on a specific task. Instead, we treat MLLMs as cognitive systems in their own right, using visual search tasks to examine whether—and *how*—their responses reflect structured visual processing similar to that observed in humans.

7 Discussion and Conclusion

Drawing on classic work in cognitive science, we systematically investigate the visual search capabilities of MLLMs. Our experiments show that the most advanced models (e.g., GPT-4o and Claude-Sonnet) closely match human behaviours including: (1) parallel performance – or “pop-out” – for search targets defined by a single primitive feature (i.e., disjunctive search), (2) capacity limits for targets that require feature binding (i.e., conjunctive search), and (3) the incorporation of natural-scene features such as a “light-from-above” prior. These findings not only help us to anticipate future perceptual behaviour of these systems, but also provides insight into the nature of their internal representations, and how these differ between models. For example, Llama 90B exhibited markedly less human-like behaviour, which we attribute to poorer overall perceptual or related auxiliary capabilities rather than differences in architecture, since smaller versions of other models we tested (e.g., GPT-4-Turbo and Claude-Haiku) were also less human-like.

Interestingly, MLLMs such as GPT-4o showed evidence of using sophisticated natural scene features, such as lighting direction, to guide visual search, and showed the best performance for objects lit from the most “surprising” direction (below), just like humans. Multimodal large language models are trained on vast, often opaque datasets. While the composition of this training data is unknown—GPT-4o’s system card (OpenAI et al., 2024), for instance, offers only high-level sourcing—much of it likely reflects real-world imagery. Our findings suggest that natural regularities, such as lighting direction, contained in training images has allowed MLLMs to incorporate such features into their object representations—as humans do.

Our main findings were also supported by our fine-grained localisation (coordinates) evaluation, measuring spatial precision, and augmented by fine-tuning and mechanistic interpretability analyses. We found that specialist training can improve conjunctive search performance, though not to the level of parallel pop-out performance, mirroring training effects in humans (Czerwinski et al., 1992). And just as basic low-level visual saliency is handled by early visual cortex in humans (Zhaoping and May, 2007) while searching for conjunctive search targets recruits higher visual cortical regions (Chelazzi et al., 1993), we found a parallel distinction between early and later network activations in Llama 90B.

Visual search tasks offer a powerful lens on MLLM behaviour, revealing both human-like attentional dynamics and model-specific processing constraints. However, our work has limitations that need to be taken into account. First of all, LLMs are known to be sensitive to the way that prompts are phrased (Alzahrani et al., 2024; Chaudhary et al., 2024) and we explored only a few prompts due to budgetary constraints (see Appendix J). Further, we limited our investigation to three visual features (colour, size, lighting direction), which could be expanded on. Future work could extend this framework to other feature dimensions—such as texture, motion, or occlusion—or investigate how models respond under compositional load or temporal constraints. As multimodal models continue to scale, cognitively informed probes like these may prove important for understanding how they represent, reason about, and act on the visual world.

References

- Wendy J. Adams. A common light-prior for visual search, shape, and reflectance judgments. *Journal of Vision*, 7(11):11, August 2007. ISSN 1534-7362. doi: 10.1167/7.11.11. URL <http://jov.arvojournals.org/article.aspx?doi=10.1167/7.11.11>.
- Jean-Baptiste Alayrac, Jeff Donahue, Pauline Luc, Antoine Miech, Iain Barr, Yana Hasson, Karel Lenc, Arthur Mensch, Katie Millican, Malcolm Reynolds, Roman Ring, Eliza Rutherford, Serkan Cabi, Tengda Han, Zhitao Gong, Sina Samangooei, Marianne Monteiro, Jacob Menick, Sebastian Borgeaud, Andrew Brock, Aida Nematzadeh, Sahand Sharifzadeh, Mikolaj Binkowski, Ricardo Barreira, Oriol Vinyals, Andrew Zisserman, and Karen Simonyan. Flamingo: a Visual Language Model for Few-Shot Learning, 2022. URL <https://arxiv.org/abs/2204.14198>. Version Number: 2.
- Norah Alzahrani, Hisham Abdullah Alyahya, Yazeed Alnumay, Sultan Alrashed, Shaykhah Alsubaie, Yusef Al-mushaykeh, Faisal Mirza, Nouf Alotaibi, Nora Altwairesh, Areeb Alowisheq, M Saiful Bari, and Haidar Khan. When benchmarks are targets: Revealing the sensitivity of large language model leaderboards, 2024. URL <https://arxiv.org/abs/2402.01781>.
- Anthropic. Claude 3.5 sonnet model card addendum, 2024. URL https://www-cdn.anthropic.com/fed9cc193a14b84131812372d8d5857f8f304c52/Model_Card_Claude_3_Addendum.pdf.
- Declan Iain Campbell, Sunayana Rane, Tyler Giallanza, C. Nicolò De Sabbata, Kia Ghods, Amogh Joshi, Alexander Ku, Steven M Frankland, Thomas L. Griffiths, Jonathan D. Cohen, and Taylor Whittington Webb. Understanding the limits of vision language models through the lens of the binding problem. In *The Thirty-eighth Annual Conference on Neural Information Processing Systems*, 2024. URL <https://openreview.net/forum?id=Q5RYn6jagC>.
- Mathilde Caron, Hugo Touvron, Ishan Misra, Hervé Jégou, Julien Mairal, Piotr Bojanowski, and Armand Joulin. Emerging properties in self-supervised vision transformers. In *Proceedings of the IEEE/CVF international conference on computer vision*, pages 9650–9660, 2021.
- Manav Chaudhary, Harshit Gupta, Savita Bhat, and Vasudeva Varma. Towards understanding the robustness of llm-based evaluations under perturbations, 2024. URL <https://arxiv.org/abs/2412.09269>.
- Leonardo Chelazzi, Earl K Miller, John Duncan, and Robert Desimone. A neural basis for visual search in inferior temporal cortex. *Nature*, 363(6427):345–347, 1993.
- Mary Czerwinski, Nancy Lightfoot, and Richard M Shiffrin. Automatization and training in visual search. *The American journal of psychology*, pages 271–315, 1992.
- Yulong Ding, Tingni Li, and Zhe Qu. Is a new feature learned behind a newly efficient color-orientation conjunction search? *Psychonomic Bulletin & Review*, 30(1):250–260, 2023.
- Zhiwei Ding, Xuezhe Ren, Erwan David, Melissa Vo, Gabriel Kreiman, and Mengmi Zhang. Efficient zero-shot visual search via target and context-aware transformer, 2022. URL <https://arxiv.org/abs/2211.13470>.
- James T Enns and Ronald A Rensink. Influence of scene-based properties on visual search. *Science*, 247(4943):721–723, 1990.
- Yash Goyal, Tejas Khot, Douglas Summers-Stay, Dhruv Batra, and Devi Parikh. Making the v in vqa matter: Elevating the role of image understanding in visual question answering, 2017. URL <https://arxiv.org/abs/1612.00837>.
- Jiayi Kuang, Ying Shen, Jingyou Xie, Haohao Luo, Zhe Xu, Ronghao Li, Yinghui Li, Xianfeng Cheng, Xika Lin, and Yu Han. Natural language understanding and inference with mllm in visual question answering: A survey. *ACM Comput. Surv.*, 57(8), March 2025. ISSN 0360-0300. doi: 10.1145/3711680. URL <https://doi.org/10.1145/3711680>.
- Junnan Li, Dongxu Li, Caiming Xiong, and Steven Hoi. BLIP: Bootstrapping Language-Image Pre-training for Unified Vision-Language Understanding and Generation, 2022. URL <https://arxiv.org/abs/2201.12086>. Version Number: 2.
- Zihao Lin, Samyadeep Basu, Mohammad Beigi, Varun Manjunatha, Ryan A Rossi, Zichao Wang, Yufan Zhou, Sriram Balasubramanian, Arman Zarei, Keivan Rezaei, et al. A survey on mechanistic interpretability for multi-modal foundation models. *arXiv preprint arXiv:2502.17516*, 2025.
- Fenglin Liu, Zheng Li, Qingyu Yin, Jinfa Huang, Jiebo Luo, Anshul Thakur, Kim Branson, Patrick Schwab, Bing Yin, Xian Wu, Yefeng Zheng, and David A. Clifton. A multimodal multidomain multilingual medical foundation model for zero shot clinical diagnosis. *npj Digital Medicine*, 8(1):86, February 2025. ISSN 2398-6352. doi: 10.1038/s41746-024-01339-7. URL <https://www.nature.com/articles/s41746-024-01339-7>.

- Haotian Liu, Chunyuan Li, Qingyang Wu, and Yong Jae Lee. Visual Instruction Tuning, 2023. URL <https://arxiv.org/abs/2304.08485>. Version Number: 2.
- Gen Luo, Ganlin Yang, Ziyang Gong, Guanzhou Chen, Haonan Duan, Erfei Cui, Ronglei Tong, Zhi Hou, Tianyi Zhang, Zhe Chen, Shenglong Ye, Lewei Lu, Jingbo Wang, Wenhai Wang, Jifeng Dai, Yu Qiao, Rongrong Ji, and Xizhou Zhu. Visual Embodied Brain: Let Multimodal Large Language Models See, Think, and Control in Spaces, May 2025. URL <http://arxiv.org/abs/2506.00123>. arXiv:2506.00123 [cs].
- Kenneth Marino, Mohammad Rastegari, Ali Farhadi, and Roozbeh Mottaghi. OK-VQA: A Visual Question Answering Benchmark Requiring External Knowledge. In *2019 IEEE/CVF Conference on Computer Vision and Pattern Recognition (CVPR)*, pages 3190–3199, Long Beach, CA, USA, June 2019. IEEE. ISBN 978-1-72813-293-8. doi: 10.1109/CVPR.2019.00331. URL <https://ieeexplore.ieee.org/document/8953725/>.
- David Marr. *Vision: a computational investigation into the human representation and processing of visual information*. Freeman, New York, 14. print edition, 2000. ISBN 978-0-7167-1567-2.
- Meta AI. Llama 3.2-90b vision model card. <https://huggingface.co/meta-llama/Llama-3.2-90B-Vision>, 2024. Accessed: 2025-05-13.
- OpenAI, :, Aaron Hurst, Adam Lerer, Adam P. Goucher, Adam Perelman, Aditya Ramesh, Aidan Clark, AJ Ostrow, Akila Welihinda, Alan Hayes, Alec Radford, Aleksander Mądry, Alex Baker-Whitcomb, Alex Beutel, Alex Borzunov, Alex Carney, Alex Chow, Alex Kirillov, Alex Nichol, Alex Paino, Alex Renzin, Alex Tachard Passos, Alexander Kirillov, Alexi Christakis, Alexis Conneau, Ali Kamali, Allan Jabri, Allison Moyer, Allison Tam, Amadou Crookes, Amin Tootoochian, Amin Tootoonchian, Ananya Kumar, Andrea Vallone, Andrej Karpathy, Andrew Braunstein, Andrew Cann, Andrew Codispoti, Andrew Galu, Andrew Kondrich, Andrew Tulloch, Andrey Mishchenko, Angela Baek, Angela Jiang, Antoine Pelisse, Antonia Woodford, Anuj Gosalia, Arka Dhar, Ashley Pantuliano, Avi Nayak, Avital Oliver, Barret Zoph, Behrooz Ghorbani, Ben Leimberger, Ben Rossen, Ben Sokolowsky, Ben Wang, Benjamin Zweig, Beth Hoover, Blake Samic, Bob McGrew, Bobby Spero, Bogo Giertler, Bowen Cheng, Brad Lightcap, Brandon Walkin, Brendan Quinn, Brian Guarraci, Brian Hsu, Bright Kellogg, Brydon Eastman, Camillo Lugaresi, Carroll Wainwright, Cary Bassin, Cary Hudson, Casey Chu, Chad Nelson, Chak Li, Chan Jun Shern, Channing Conger, Charlotte Barette, Chelsea Voss, Chen Ding, Cheng Lu, Chong Zhang, Chris Beaumont, Chris Hallacy, Chris Koch, Christian Gibson, Christina Kim, Christine Choi, Christine McLeavey, Christopher Hesse, Claudia Fischer, Clemens Winter, Coley Czarnecki, Colin Jarvis, Colin Wei, Constantin Koumouzelis, Dane Sherburn, Daniel Kappler, Daniel Levin, Daniel Levy, David Carr, David Farhi, David Mely, David Robinson, David Sasaki, Denny Jin, Dev Valladares, Dimitris Tsipras, Doug Li, Duc Phong Nguyen, Duncan Findlay, Edede Oiwoh, Edmund Wong, Ehsan Asdar, Elizabeth Proehl, Elizabeth Yang, Eric Antonow, Eric Kramer, Eric Peterson, Eric Sigler, Eric Wallace, Eugene Brevdo, Evan Mays, Farzad Khorasani, Felipe Petroski Such, Filippo Raso, Francis Zhang, Fred von Lohmann, Freddie Sulit, Gabriel Goh, Gene Oden, Geoff Salmon, Giulio Starace, Greg Brockman, Hadi Salman, Haiming Bao, Haitang Hu, Hannah Wong, Haoyu Wang, Heather Schmidt, Heather Whitney, Heewoo Jun, Hendrik Kirchner, Henrique Ponde de Oliveira Pinto, Hongyu Ren, Huiwen Chang, Hyung Won Chung, Ian Kivlichen, Ian O’Connell, Ian O’Connell, Ian Osband, Ian Silber, Ian Sohl, Ibrahim Okuyucu, Ikai Lan, Ilya Kostrikov, Ilya Sutskever, Ingmar Kanitscheider, Ishaan Gulrajani, Jacob Coxon, Jacob Menick, Jakub Pachocki, James Aung, James Betker, James Crooks, James Lennon, Jamie Kiros, Jan Leike, Jane Park, Jason Kwon, Jason Phang, Jason Teplitz, Jason Wei, Jason Wolfe, Jay Chen, Jeff Harris, Jenia Varavva, Jessica Gan Lee, Jessica Shieh, Ji Lin, Jiahui Yu, Jiayi Weng, Jie Tang, Jieqi Yu, Joanne Jang, Joaquin Quinonero Candela, Joe Beutler, Joe Landers, Joel Parish, Johannes Heidecke, John Schulman, Jonathan Lachman, Jonathan McKay, Jonathan Uesato, Jonathan Ward, Jong Wook Kim, Joost Huizinga, Jordan Sitkin, Jos Kraaijeveld, Josh Gross, Josh Kaplan, Josh Snyder, Joshua Achiam, Joy Jiao, Joyce Lee, Juntang Zhuang, Justyn Harriman, Kai Fricke, Kai Hayashi, Karan Singhal, Katy Shi, Kavin Karthik, Kayla Wood, Kendra Rimbach, Kenny Hsu, Kenny Nguyen, Keren Gu-Lemberg, Kevin Button, Kevin Liu, Kiel Howe, Krithika Muthukumar, Kyle Luther, Lama Ahmad, Larry Kai, Lauren Itow, Lauren Workman, Leher Pathak, Leo Chen, Li Jing, Lia Guy, Liam Fedus, Liang Zhou, Lien Mamitsuka, Lilian Weng, Lindsay McCallum, Lindsey Held, Long Ouyang, Louis Feuvrier, Lu Zhang, Lukas Kondraciuk, Lukasz Kaiser, Luke Hewitt, Luke Metz, Lyric Doshi, Mada Aflak, Maddie Simens, Madelaine Boyd, Madeleine Thompson, Marat Dukhan, Mark Chen, Mark Gray, Mark Hudnall, Marvin Zhang, Marwan Aljubeih, Mateusz Litwin, Matthew Zeng, Max Johnson, Maya Shetty, Mayank Gupta, Meghan Shah, Mehmet Yatbaz, Meng Jia Yang, Mengchao Zhong, Mia Glaese, Mianna Chen, Michael Janner, Michael Lampe, Michael Petrov, Michael Wu, Michele Wang, Michelle Fradin, Michelle Pokrass, Miguel Castro, Miguel Oom Temudo de Castro, Mikhail Pavlov, Miles Brundage, Miles Wang, Minal Khan, Mira Murati, Mo Bavarian, Molly Lin, Murat Yesildal, Nacho Soto, Natalia Gimelshein, Natalie Cone, Natalie Staudacher, Natalie Summers, Natan LaFontaine, Neil Chowdhury, Nick Ryder, Nick Stathas, Nick Turley, Nik Tezak, Niko Felix, Nithanth Kudige, Nitish Keskar, Noah Deutsch, Noel Bundick, Nora Puckett, Ofir Nachum, Ola Okelola, Oleg Boiko, Oleg Murk, Oliver Jaffe, Olivia Watkins, Olivier Godement, Owen Campbell-Moore, Patrick Chao, Paul McMillan, Pavel Belov, Peng Su, Peter Bak, Peter Bakum, Peter Deng, Peter Dolan, Peter Hoeschele, Peter

- Welinder, Phil Tillet, Philip Pronin, Philippe Tillet, Prafulla Dhariwal, Qiming Yuan, Rachel Dias, Rachel Lim, Rahul Arora, Rajan Troll, Randall Lin, Rapha Gontijo Lopes, Raul Puri, Reah Miyara, Reimar Leike, Renaud Gaubert, Reza Zamani, Ricky Wang, Rob Donnelly, Rob Honsby, Rocky Smith, Rohan Sahai, Rohit Ramchandani, Romain Huet, Rory Carmichael, Rowan Zellers, Roy Chen, Ruby Chen, Ruslan Nigmatullin, Ryan Cheu, Saachi Jain, Sam Altman, Sam Schoenholz, Sam Toizer, Samuel Miserendino, Sandhini Agarwal, Sara Culver, Scott Ethersmith, Scott Gray, Sean Grove, Sean Metzger, Shamez Hermani, Shantanu Jain, Shengjia Zhao, Sherwin Wu, Shino Jomoto, Shirong Wu, Shuaiqi, Xia, Sonia Phene, Spencer Papay, Srinivas Narayanan, Steve Coffey, Steve Lee, Stewart Hall, Suchir Balaji, Tal Broda, Tal Stramer, Tao Xu, Tarun Gogineni, Taya Christianson, Ted Sanders, Tejal Patwardhan, Thomas Cunningham, Thomas Degry, Thomas Dimson, Thomas Raoux, Thomas Shadwell, Tianhao Zheng, Todd Underwood, Todor Markov, Toki Sherbakov, Tom Rubin, Tom Stasi, Tomer Kaftan, Tristan Heywood, Troy Peterson, Tyce Walters, Tyna Eloundou, Valerie Qi, Veit Moeller, Vinnie Monaco, Vishal Kuo, Vlad Fomenko, Wayne Chang, Weiyi Zheng, Wenda Zhou, Wesam Manassra, Will Sheu, Wojciech Zaremba, Yash Patil, Yilei Qian, Yongjik Kim, Youlong Cheng, Yu Zhang, Yuchen He, Yuchen Zhang, Yujia Jin, Yunxing Dai, and Yury Malkov. Gpt-4o system card, 2024. URL <https://arxiv.org/abs/2410.21276>.
- Julius Orłowski, Christian Beissel, Friederike Rohn, Yair Adato, Hermann Wagner, and Ohad Ben-Shahar. Visual pop-out in barn owls: Human-like behavior in the avian brain. *Journal of Vision*, 15(14):4, October 2015. ISSN 1534-7362. doi: 10.1167/15.14.4. URL <http://jov.arvojournals.org/article.aspx?doi=10.1167/15.14.4>.
- Michael J. Proulx. Size Matters: Large Objects Capture Attention in Visual Search. *PLoS ONE*, 5(12):e15293, December 2010. ISSN 1932-6203. doi: 10.1371/journal.pone.0015293. URL <https://dx.plos.org/10.1371/journal.pone.0015293>.
- Alec Radford, Jong Wook Kim, Chris Hallacy, Aditya Ramesh, Gabriel Goh, Sandhini Agarwal, Girish Sastry, Amanda Askell, Pamela Mishkin, Jack Clark, Gretchen Krueger, and Ilya Sutskever. Learning Transferable Visual Models From Natural Language Supervision, 2021. URL <https://arxiv.org/abs/2103.00020>. Version Number: 1.
- Maithra Raghu, Thomas Unterthiner, Simon Kornblith, Chiyuan Zhang, and Alexey Dosovitskiy. Do vision transformers see like convolutional neural networks? *Advances in neural information processing systems*, 34:12116–12128, 2021.
- Adam Reichenenthal, Mor Ben-Tov, Ohad Ben-Shahar, and Ronen Segev. What pops out for you pops out for fish: Four common visual features. *Journal of Vision*, 19(1):1, January 2019. ISSN 1534-7362. doi: 10.1167/19.1.1. URL <http://jov.arvojournals.org/article.aspx?doi=10.1167/19.1.1>.
- Manoosh Samiei and James J. Clark. Target features affect visual search, a study of eye fixations, 2022. URL <https://arxiv.org/abs/2209.13771>.
- Missie Smith, Jillian Streeter, Gary Burnett, and Joseph L Gabbard. Visual search tasks: the effects of head-up displays on driving and task performance. In *Proceedings of the 7th international conference on Automotive User Interfaces and Interactive Vehicular Applications*, pages 80–87, 2015.
- Yuling Su, Yunpeng Lai, Wanyi Huang, Wei Tan, Zhe Qu, and Yulong Ding. Short-term perceptual learning in visual conjunction search. *Journal of Experimental Psychology: Human Perception and Performance*, 40(4):1415, 2014.
- Fermín Travi, Gonzalo Ruarte, Gaston Bujia, and Juan Esteban Kamienkowski. Visions: Visual search in natural scenes benchmark. In S. Koyejo, S. Mohamed, A. Agarwal, D. Belgrave, K. Cho, and A. Oh, editors, *Advances in Neural Information Processing Systems*, volume 35, pages 11987–12000. Curran Associates, Inc., 2022. URL https://proceedings.neurips.cc/paper_files/paper/2022/file/4ea14e6090343523ddcd5d3ca449695f-Paper-Datasets_and_Benchmarks.pdf.
- Anne M. Treisman and Garry Gelade. A feature-integration theory of attention. *Cognitive Psychology*, 12(1):97–136, January 1980. ISSN 00100285. doi: 10.1016/0010-0285(80)90005-5. URL <https://linkinghub.elsevier.com/retrieve/pii/0010028580900055>.
- Jeremy M. Wolfe. Guided Search 2.0 A revised model of visual search. *Psychonomic Bulletin & Review*, 1(2):202–238, June 1994. ISSN 1069-9384, 1531-5320. doi: 10.3758/BF03200774. URL <http://link.springer.com/10.3758/BF03200774>.
- Jeremy M. Wolfe. What Can 1 Million Trials Tell Us About Visual Search? *Psychological Science*, 9(1):33–39, January 1998. ISSN 0956-7976, 1467-9280. doi: 10.1111/1467-9280.00006. URL <https://journals.sagepub.com/doi/10.1111/1467-9280.00006>.
- Jeremy M. Wolfe. Visual Search: How Do We Find What We Are Looking For? *Annual Review of Vision Science*, 6(1):539–562, September 2020. ISSN 2374-4642, 2374-4650. doi: 10.1146/annurev-vision-091718-015048. URL <https://www.annualreviews.org/doi/10.1146/annurev-vision-091718-015048>.

- Jeremy M. Wolfe and Todd S. Horowitz. What attributes guide the deployment of visual attention and how do they do it? *Nature Reviews Neuroscience*, 5(6):495–501, June 2004. ISSN 1471-003X, 1471-0048. doi: 10.1038/nrn1411. URL <https://www.nature.com/articles/nrn1411>.
- Jeremy M. Wolfe, Evan M. Palmer, and Todd S. Horowitz. Reaction time distributions constrain models of visual search. *Vision Research*, 50(14):1304–1311, June 2010. ISSN 00426989. doi: 10.1016/j.visres.2009.11.002. URL <https://linkinghub.elsevier.com/retrieve/pii/S0042698909005021>.
- Penghao Wu and Saining Xie. V*: Guided visual search as a core mechanism in multimodal llms, 2023. URL <https://arxiv.org/abs/2312.14135>.
- Qi Wu, Damien Teney, Peng Wang, Chunhua Shen, Anthony Dick, and Anton van den Hengel. Visual question answering: A survey of methods and datasets. *Computer Vision and Image Understanding*, 163:21–40, 2017. ISSN 1077-3142. doi: <https://doi.org/10.1016/j.cviu.2017.05.001>. URL <https://www.sciencedirect.com/science/article/pii/S1077314217300772>. Language in Vision.
- Xiang Yue, Yuansheng Ni, Tianyu Zheng, Kai Zhang, Ruoqi Liu, Ge Zhang, Samuel Stevens, Dongfu Jiang, Weiming Ren, Yuxuan Sun, Cong Wei, Botao Yu, Ruibin Yuan, Renliang Sun, Ming Yin, Boyuan Zheng, Zhenzhu Yang, Yibo Liu, Wenhao Huang, Huan Sun, Yu Su, and Wenhua Chen. MMMU: A Massive Multi-Discipline Multimodal Understanding and Reasoning Benchmark for Expert AGI. In *2024 IEEE/CVF Conference on Computer Vision and Pattern Recognition (CVPR)*, pages 9556–9567, Seattle, WA, USA, June 2024. IEEE. ISBN 9798350353006. doi: 10.1109/CVPR52733.2024.00913. URL <https://ieeexplore.ieee.org/document/10656299/>.
- Matthew D Zeiler and Rob Fergus. Visualizing and understanding convolutional networks. In *European conference on computer vision*, pages 818–833. Springer, 2014.
- Li Zhaoping and Keith A May. Psychophysical tests of the hypothesis of a bottom-up saliency map in primary visual cortex. *PLoS Computational Biology*, 3(4):e62, 2007.

A Fine-Grained Localisation Results

Here we present the results for the fine-grained localisation ("coordinates") evaluation. The addition of coordinates (instead of just the Cells variant) allows us to capture different levels of visual understanding. *Cells* requires only a coarse-grained ability to locate the object, while *Coordinates* demands fine-grained spatial precision. Although classical visual search studies typically focus on detection, we argue that localisation is especially relevant in the context of MLLMs, which are intended to act on or reason over visual scenes—tasks that depend on accurate visual perception. In both *Cells* and *Coordinates* conditions, correct localisation is defined by the centre of the target object. For *Cells*, this determines the ground-truth grid cell label; for *Coordinates*, it serves as the reference point for Euclidean distance evaluation.

We note that Claude Sonnet frequently declined to provide coordinates in this task. In these cases, it instead responded that no target could be identified. We treat such refusals as maximum reasonable localisation error trials ($\sqrt{400^2 + 400^2} \approx 566$ pixels). Similarly, Llama 90B would often report coordinates outside of the 400×400 range. Here we score models normally according to Euclidean distance. We examine the phenomena of invalid responses in more detail in Appendix D.

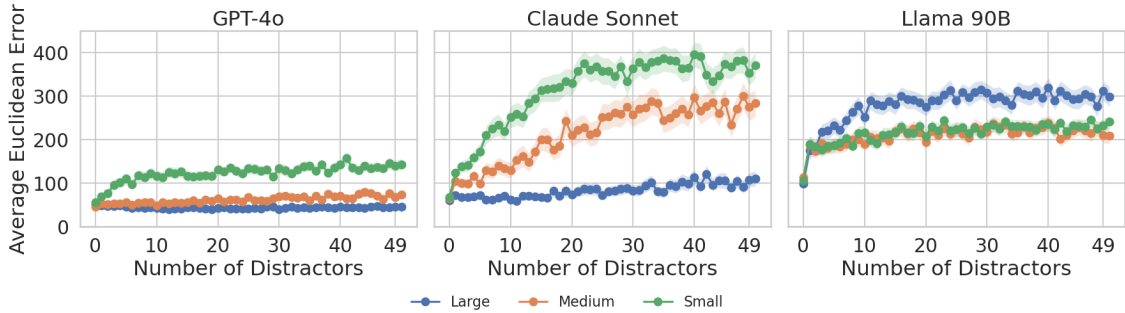


Figure 8: Results for Circle Sizes on Coordinates. The shaded region denotes the 95% confidence interval.

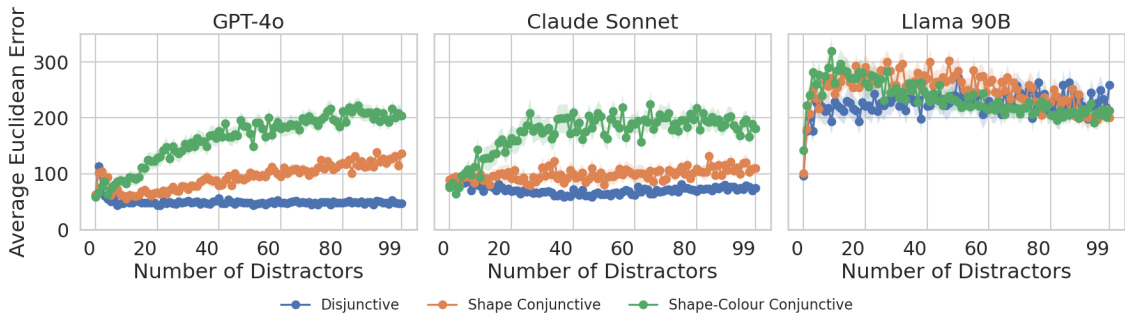


Figure 9: Results for the 2Among5 task — Coordinates mode. The shaded region denotes the 95% confidence interval.

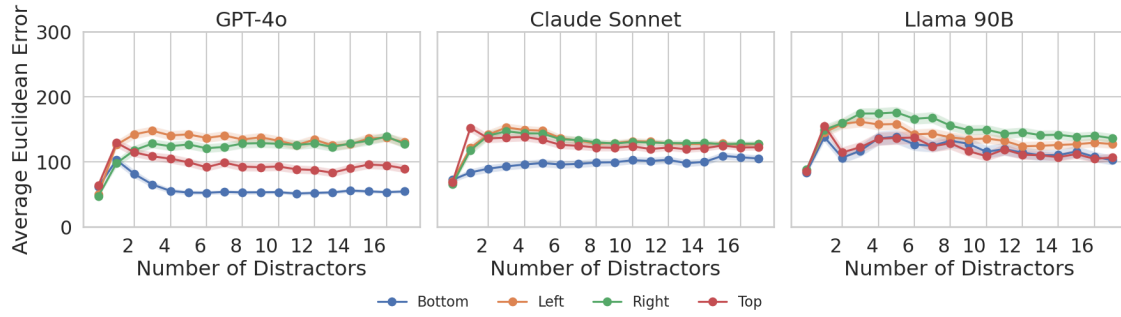


Figure 10: Results for the Light Priors task — Coordinates mode. The shaded region denotes the 95% confidence interval.

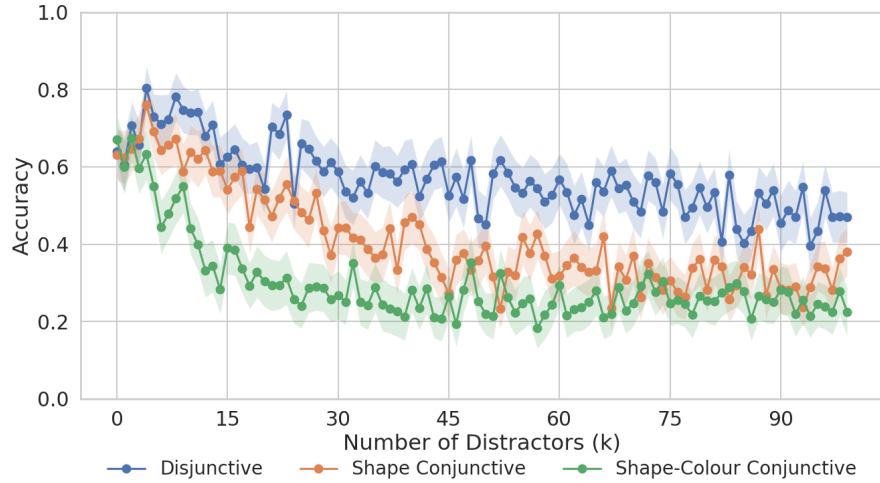
B Results for Additional Models

Due to space constraints it was not possible to provide figures for each model tested on each task within the main body of the paper. In this section we provide the results for other tested models and compare the results to humans and other models. We principally compare against smaller models (or earlier models in the same families) as those in the main paper; intending to enable a comparison of how visual search mechanisms change with scale. Therefore we include GPT-4-Turbo, Claude-Haiku (3.5), and Llama (3.2) 11B. With the exception of GPT-4-Turbo, these models perform significantly worse than their larger versions, and quickly fall to chance level performance, even in Disjunctive cases, or other variants where pop-out effects were present.

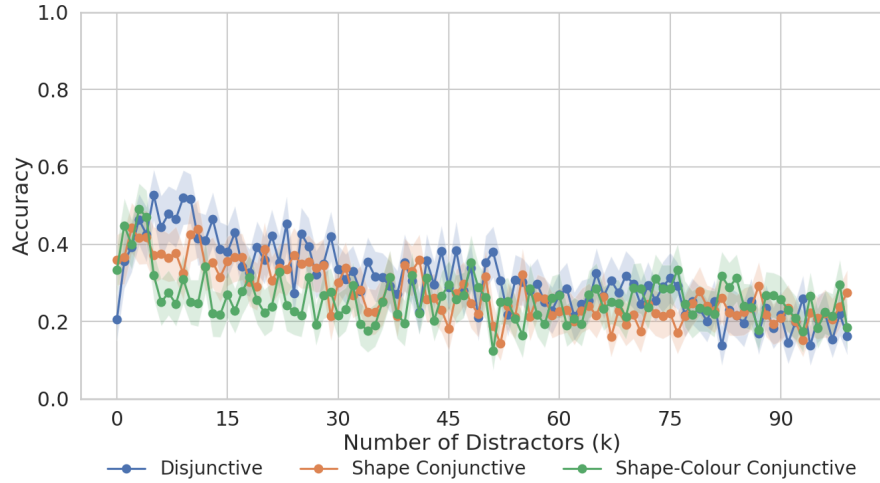
Two Among Five additional Results Figures 11 and 12 detail the results for our smaller models. For Claude Haiku and Llama 11B in the Cells evaluation there is little difference between their performance and effectively random chance. GPT-4-Turbo on the other hand performs better, in similar pattern to the MLLMs in the main paper and humans, but with reduced performance. In the Coordinates evaluation, all three perform only marginally better in the disjunctive setting, though the distinction can become clearer at a higher set-size.

Light Priors Figures 13 and 14 detail the results for GPT-4-Turbo, Claude-Haiku, and Llama 11B in the Light Priors task, for both the Cells and Coordinates Evaluation. Similar to the Two Among Five results, these less capable models perform much worse than the models in the main body of the paper. Notably, Claude-Haiku, manages to robustly attain worse-than-chance performance in the Cells evaluation. Upon inspection it became evident that Haiku was selecting invalid options such as “Cell (2,4)” and “Cell (2,3)” frequently. It is unclear what caused this specifically for the Light Priors task and Claude-Haiku, when other models and tasks were largely unaffected.

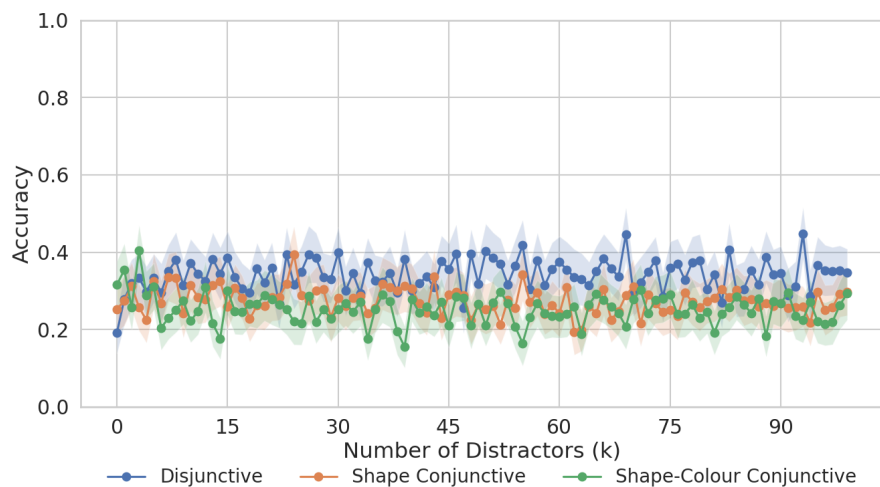
Circle Sizes Figures 15 and 16 detail the results for our smaller models on the Circle Sizes task, again for both Cells and Coordinates evaluations. Once again, we see substantially worse performance compared to the larger models in the main paper, with Llama 11B in particular not performing better than chance, and Haiku and GPT-4-turbo only performing marginally better than chance for the Large variant of the task. In terms of coordinates set up, GPT-4-Turbo and Claude-Haiku again perform slightly better in the Large variant.



(a) GPT-4-Turbo

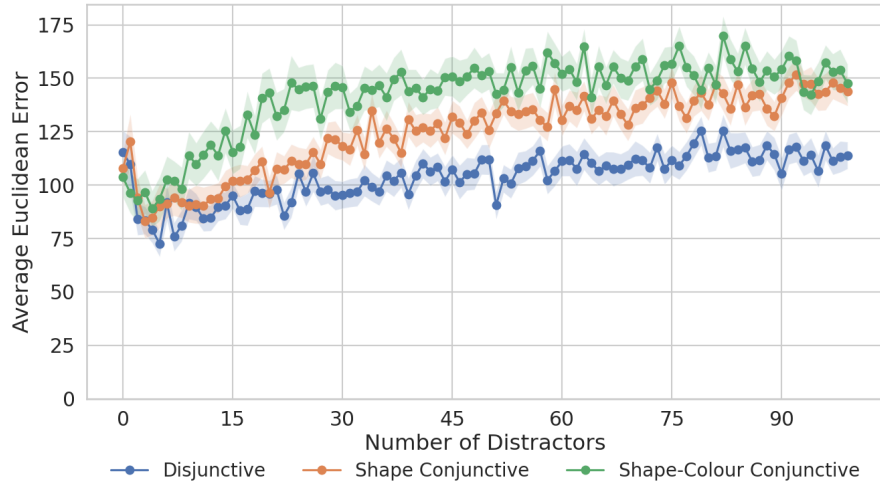


(b) Claude Haiku

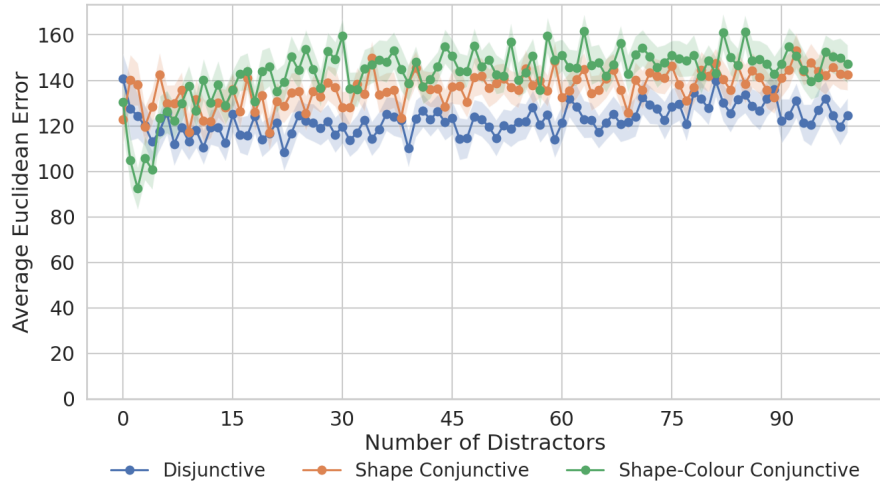


(c) Llama 11B

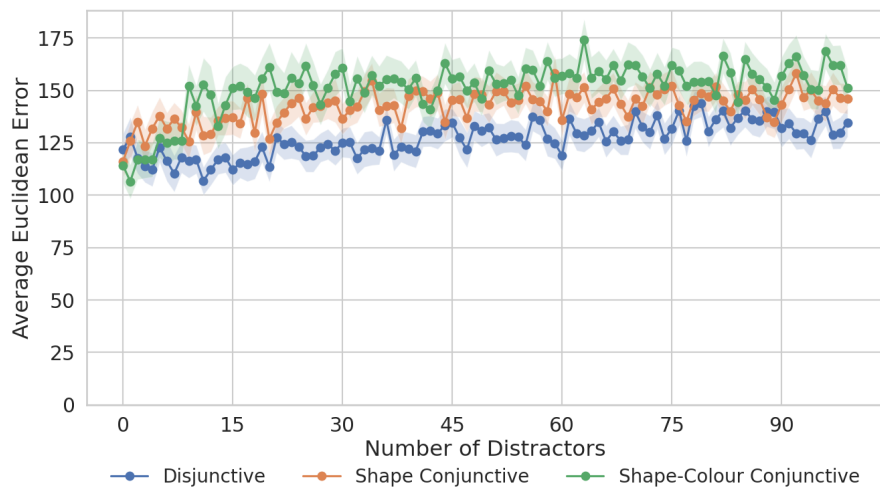
Figure 11: Results for the 2Among5 task using Cells modes for our three smaller or earlier models. The shaded region denotes the 95% confidence interval.



(a) GPT-4-Turbo

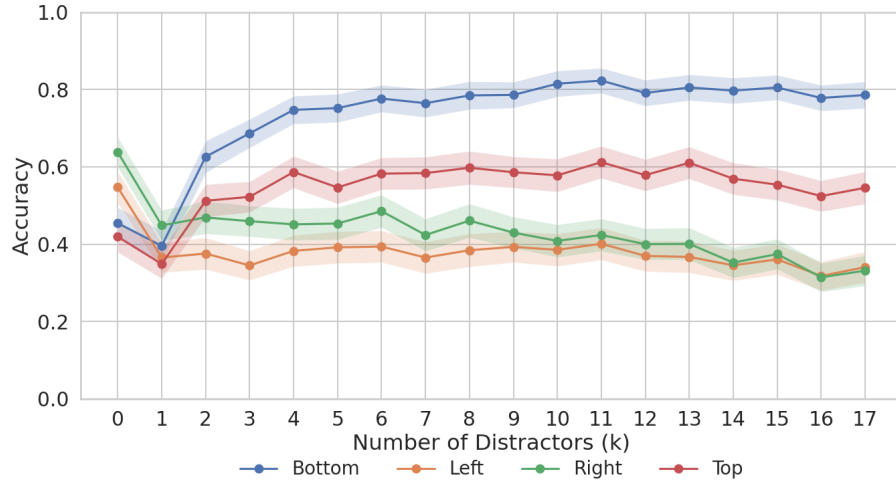


(b) Claude Haiku

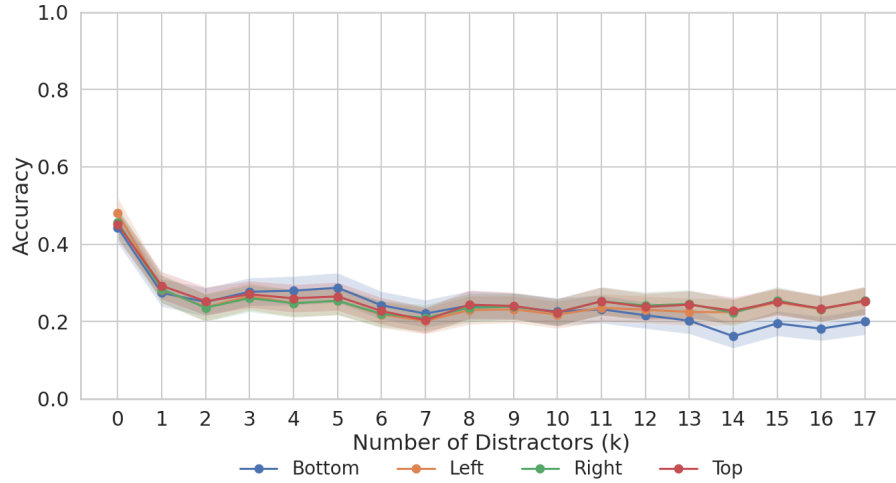


(c) Llama 11B

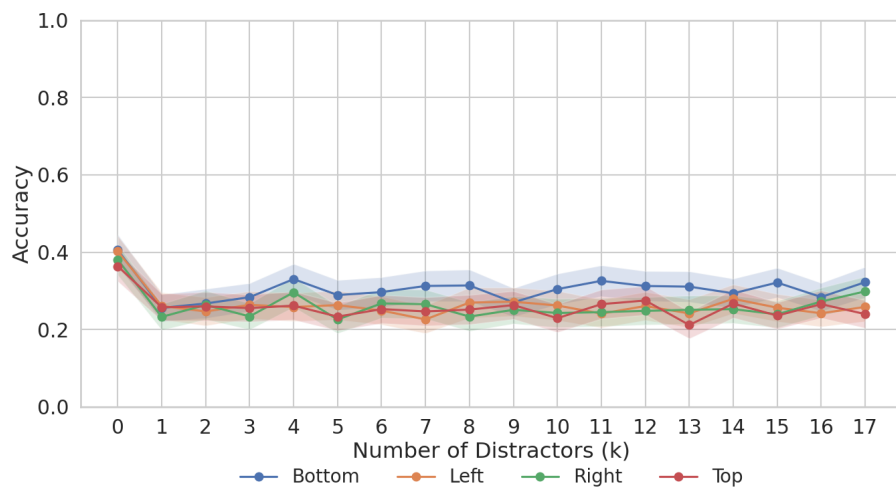
Figure 12: Results for the 2Among5 task using Coordinates modes for our three smaller or earlier models. The shaded region denotes the 95% confidence interval.



(a) GPT-4-Turbo

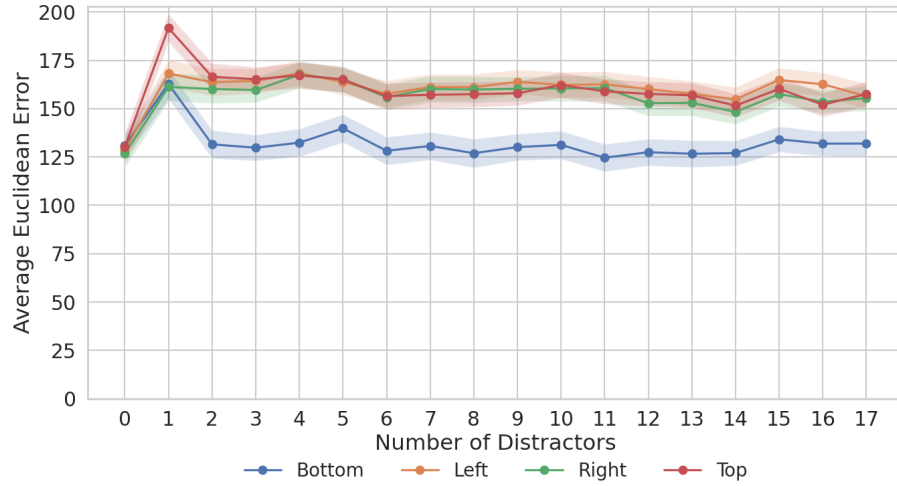


(b) Claude Haiku

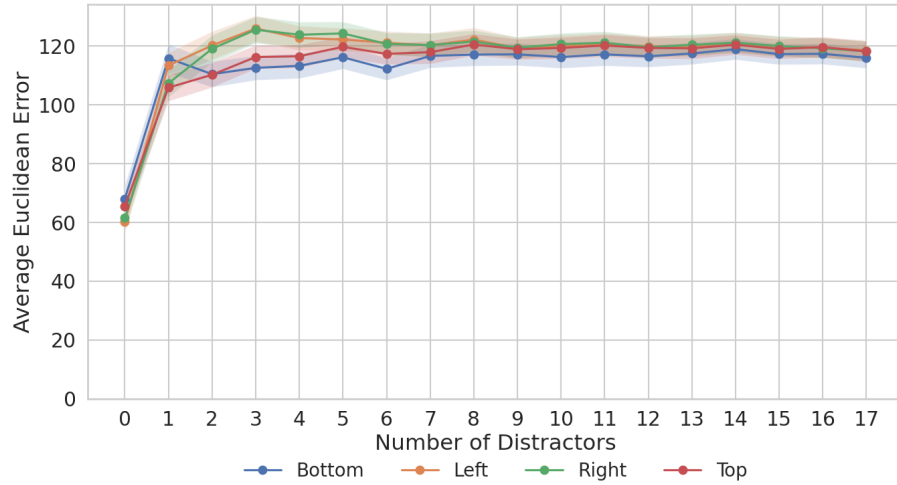


(c) Llama 11B

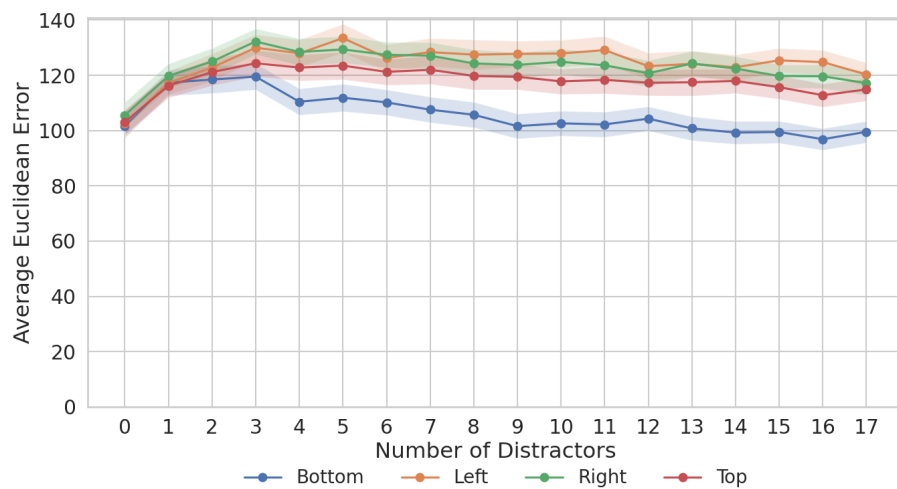
Figure 13: Results for the Light Priors task using Cells modes for our three smaller or earlier models. The shaded region denotes the 95% confidence interval.



(a) GPT-4-Turbo

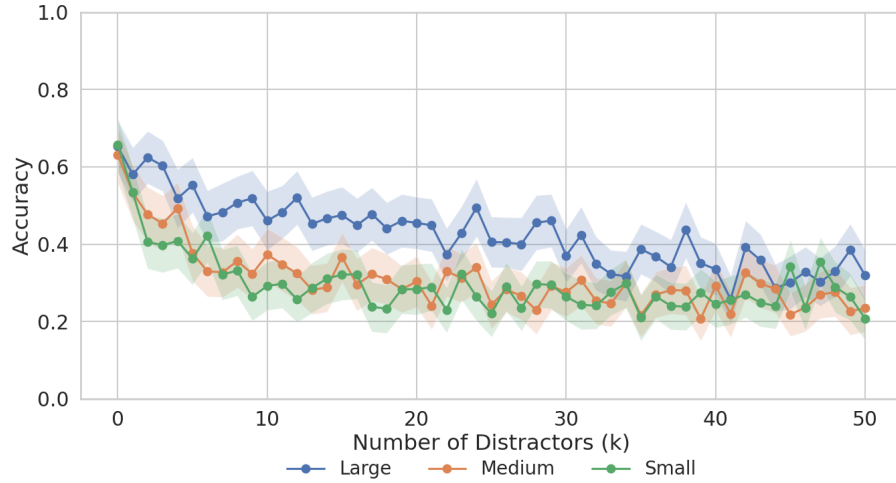


(b) Claude Haiku

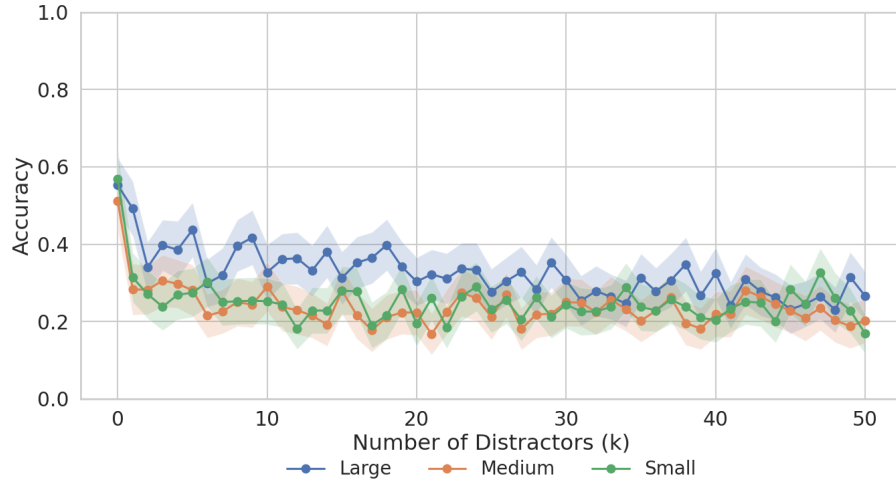


(c) Llama 11B

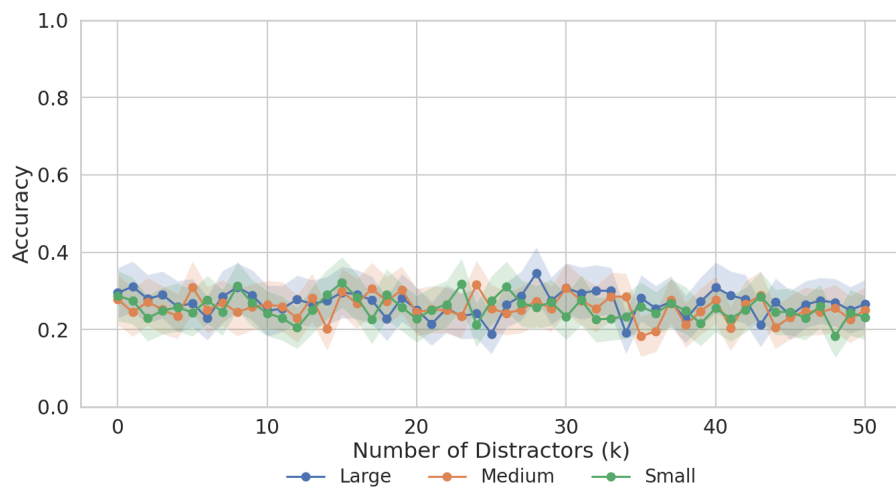
Figure 14: Results for the Light Priors task using Coordinates modes for our three smaller or earlier models. The shaded region denotes the 95% confidence interval.



(a) GPT-4-Turbo

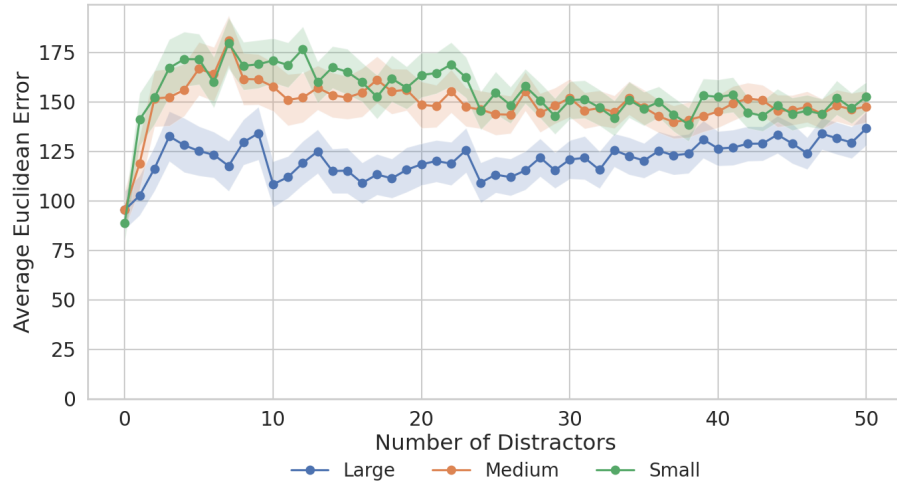


(b) Claude Haiku

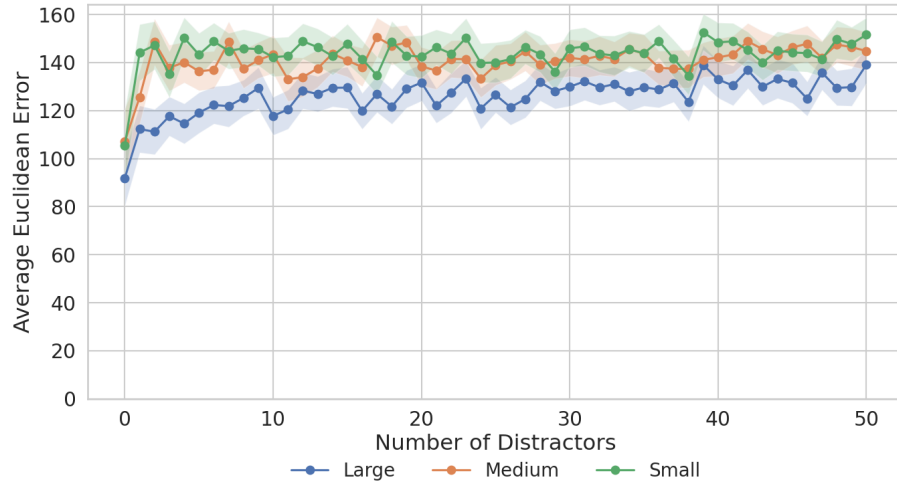


(c) Llama 11B

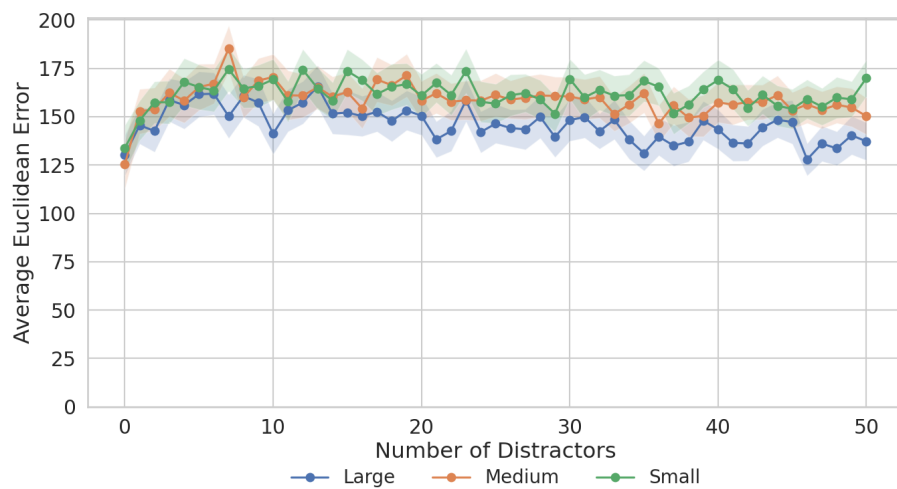
Figure 15: Results for the Circle Sizes task using Cells modes for our three smaller or earlier models. The shaded region denotes the 95% confidence interval.



(a) GPT-4-Turbo



(b) Claude Haiku



(c) Llama 11B

Figure 16: Results for the Circle Sizes task using Coordinates modes for our three smaller or earlier models. The shaded region denotes the 95% confidence interval.

C Model Details

In this section we provide more detail on the specific models used, hyper-parameters and overall settings. Most hyper-parameters were left at their default settings in order to be the most “out-of-the-box” representation of each model. We did set for each model a temperature of 0.0 to ensure as deterministic a response as possible. The specific versions of models used are described in Table 1.

When running experiments for the Llama models we utilised a pre-existing implementation via Hugging Face Transformers⁵. Models were instantiated with `MllamaForConditionalGeneration` and paired with their corresponding `AutoProcessor`. All inference ran on GPU using automatic device mapping and `bfloat16` precision. Crucially, we did not enable sampling (`do_sample=False` by default), so generation was greedy — i.e., the model always selected the highest-probability token at each step. Thus, the model’s output was deterministic and equivalent to using temperature 0.

Table 1: Language models and their specific versions used in our experiments.

Model	Version Used
GPT-4o	gpt-4o-2024-08-06
GPT-4-Turbo	gpt-4-turbo-2024-04-09
Claude Sonnet	claude-3-5-sonnet-20241022)
Claude Haiku	claude-3-5-haiku-20241022
Llama 90B	Meta LLaMA 3.2 90B
Llama 11B	Meta LLaMa 3.2 11B

D Invalid Responses

Despite efforts to ensure models responded appropriately, the stochastic nature of MLLMs led to invalid or nonsensical results. For the Cells evaluations, these were infrequent, and detailed in Tables 4, 5, 6, 7, 8, and 9. To summarise, in 2 Among 5, All models would occasionally respond with invalid Cells (such as Cell (2,3)). The biggest offender was Claude-Haiku, however, GPT-4o and Claude-Sonnet would also do this between 3 and 5% of the time in some variations. For Light Priors, Claude-Haiku was again the biggest culprit, in some cases providing invalid responses over 78% of the time. Again, GPT-4o would do this over 8% of the time in the Top and Bottom variations—interesting because it performed better in these variants overall. For Circle Sizes, GPT-4o responded invalidly for 2.78% of instances for the small variation, while Llama 90B did the same for over 1% of cases in all variations. Again, Haiku frequently provided invalid responses (between 4.49 and 13.18 %).

In the Coordinates evaluations, we can distinguish between models refusing to provide coordinates, and providing implausible coordinates outside of the image size.

In 2 Among 5, we see models failing to provide coordinates as outlined in Table 2. Again, Sonnet is the largest contributor, rising to over 8% invalid in the Cojunctive variant. Other models are all less than 1%.

Llama 90B is the only model to provide coordinates outside of the expected range (outside the 400x400 pixel range). Strangely, it does this more frequently for the easier Disjunctive variant (42.16%) than the more difficult Shape Conjunctive (39.34%) or Shape-Colour Conjunctive (18.2%) variations.

Table 2: Rate of failure to provide coordinates (%) by model and logical condition in the 2 Among 5 task.

Model	Disjunctive	Shape Conjunctive	Shape-Colour Conjunctive
claude-haiku	0.00	0.00	0.00
claude-sonnet	0.17	3.21	8.34
gpt-4-turbo	0.00	0.00	0.00
gpt-4o	0.03	0.39	0.91
llama11B	0.02	0.05	0.18
llama90B	0.00	0.00	0.01

⁵<https://huggingface.co/docs/transformers/index>

For the Light Priors task, we detail failure to provide coordinate rates in Table 3. Models generally provided coordinates in this task, with no model ever approaching even a 1% failure rate. Llama 90B continues to provide coordinates that do not make sense given the question. Returning coordinates outside of the range mostly frequently in Bottom (9.58%) and Top (6.86%), but also present in Right (0.93% and Left (1.02%). This is odd, as generally Llama 90B performs much better on the Vertical (Top and Bottom) stimuli, but when mistakes are made, it’s frequently because of this coordinate error.

Table 3: Rate of failure to provide coordinates (%) by model and lighting direction in the Light Priors Task.

Model	Bottom	Left	Right	Top
claude-haiku	0.00	0.00	0.00	0.00
claude-sonnet	0.00	0.00	0.00	0.00
gpt-4-turbo	0.00	0.00	0.00	0.00
gpt-4o	0.09	0.02	0.01	0.16
llama11B	0.00	0.00	0.00	0.00
llama90B	0.00	0.00	0.00	0.00

In the Circle Sizes task, Claude would fail to provide a coordinate pair in 2.7% (Large), 23.42% (Medium), and 39.2% (Small). GPT-4o failed to provide coordinates in 0.24% of Small instances. All other models always provided coordinates.

Llama 90B would again often provide coordinates outside of the expected range. Again, more often in the easier Large variation (52.7% of the time) than the Medium (10.56%) or Small variations (1.6%). It is unclear why Llama 90B responded like this. No other model ever provided coordinates outside of the 400x400 range in this task.

For the finetuned models described in Section 4 and Appendix H, the number of invalid responses decayed as finetuning went on, eventually reaching 0 invalid responses at n=100 and n=1000.

E Spatial Bias

In this section we investigate the spatial bias and preferences exhibited by models in our experiments. For each experiment in the Cells evaluation we break down performance by cell category (i.e., which quadrant of the screen the target was in). We present Precision, Recall, and the Selection proportion (i.e., in what proportion of trials did the model select this cell?).

Overall we uncover that different models have different tendencies to pick particular cells more frequently than others, even though the set of tasks had approximately an equal number of trials where the target was in each quadrant. However, these preferences or biases do not seem to carry over from task to task.

We also observed small elements of spatial bias in the human results (See tables in I.3. This makes more sense as the humans were exposed the stimulus for a short period of time and consistent search strategies (e.g., top-down) would lead to apparent spatial bias if there wasn’t sufficient time to find the target. However, MLLMs were not subject to these timing constraints and are simply required to transform the input image-prompt pair into an answer.

E.1 2 Among 5

The spatial bias results for GPT-4o, Claude-Sonnet, and Llama 90B are presented in Table 4. From the selection proportions it is apparent that GPT-4o has a preference for selecting the top-right corner, and to some extent, the bottom right quadrant. The top-right preference is most clear in the hardest task, Shape-Colour Conjunctive, where GPT-4o selects it 47.9% of the time. Conversely, Claude-sonnet clearly prefers the bottom-left quadrant, and in the two harder task variants (Shape Conjunctive and Shape-Colour Conjunctive) it selects it over 50% of the time. Finally, Llama 90B also exhibits a preference for the bottom-right quadrant. The spatial bias results for the additional models are provided in Table 5. Here all models are heavily biased towards the bottom right quadrant. This likely explains these models lower performance. It is unclear where this preference has come from.

Table 4: Model classification performance and predicted proportions on the 2Among5 task GPT-4o, Claude-Sonnet, and Llama 90B. “Sel” denotes the proportion of predictions (in %) assigned to each label.

(a) GPT-4o

Label	Disjunctive			Shape Conjunctive			Shape-Colour Conjunctive		
	Prec	Rec	Sel	Prec	Rec	Sel	Prec	Rec	Sel
Top Left	0.89	0.78	22.1	0.94	0.30	8.0	0.50	0.23	11.6
Top Right	0.76	0.98	32.9	0.58	0.70	30.8	0.36	0.68	47.9
Bottom Left	0.90	0.82	23.0	0.71	0.48	16.8	0.48	0.37	19.0
Bottom Right	0.92	0.81	21.2	0.47	0.75	38.6	0.49	0.36	17.9
Invalid			0.80			5.80			3.54

(b) Claude-Sonnet

Label	Disjunctive			Shape Conjunctive			Shape-Colour Conjunctive		
	Prec	Rec	Sel	Prec	Rec	Sel	Prec	Rec	Sel
Top Left	0.96	0.26	6.8	0.93	0.21	5.7	0.54	0.17	7.7
Top Right	0.61	0.75	31.2	0.59	0.58	24.7	0.47	0.28	15.1
Bottom Left	0.58	0.94	40.5	0.46	0.94	50.6	0.32	0.74	58.1
Bottom Right	0.85	0.76	21.5	0.84	0.63	18.4	0.46	0.28	15.1
Invalid			0.02			0.53			3.90

(c) LLaMA 90B

Label	Disjunctive			Shape Conjunctive			Shape-Colour Conjunctive		
	Prec	Rec	Sel	Prec	Rec	Sel	Prec	Rec	Sel
Top Left	0.71	0.48	17.3	0.79	0.28	9.0	0.33	0.46	34.8
Top Right	0.48	0.21	11.0	0.42	0.09	5.5	0.35	0.04	3.1
Bottom Left	0.65	0.64	24.9	0.52	0.47	22.7	0.29	0.25	22.2
Bottom Right	0.45	0.88	46.8	0.35	0.82	56.9	0.30	0.48	39.4
Invalid			0.07			5.83			0.56

Table 5: Classification performance and predicted proportions on the 2Among5 Task for GPT-4-Turbo, Claude-Haiku, and Llama 11B. “Sel” indicates the proportion of model predictions assigned to each label (in %).

(a) GPT-4-turbo

Label	Disjunctive			Shape Conjunctive			Shape-Colour Conjunctive		
	Prec	Rec	Sel	Prec	Rec	Sel	Prec	Rec	Sel
Top Left	0.93	0.20	5.3	0.88	0.11	3.1	0.72	0.05	1.7
Top Right	0.60	0.63	26.9	0.65	0.21	8.1	0.42	0.17	9.9
Bottom Left	0.75	0.54	18.3	0.56	0.47	20.7	0.32	0.41	32.6
Bottom Right	0.46	0.93	48.0	0.32	0.88	66.7	0.27	0.58	52.8
Invalid			1.49			1.43			3.02

(b) Claude-Haiku

Label	Disjunctive			Shape Conjunctive			Shape-Colour Conjunctive		
	Prec	Rec	Sel	Prec	Rec	Sel	Prec	Rec	Sel
Top Left	1.00	0.07	1.7	1.00	0.03	0.7	0.93	0.01	0.3
Top Right	0.46	0.09	4.8	0.50	0.03	1.6	0.34	0.01	0.7
Bottom Left	0.68	0.25	9.4	0.68	0.18	6.6	0.50	0.05	2.5
Bottom Right	0.29	0.85	69.9	0.26	0.88	81.8	0.25	0.99	95.9
Invalid			14.29			9.33			0.57

(c) LLaMA 11B

Label	Disjunctive			Shape Conjunctive			Shape-Colour Conjunctive		
	Prec	Rec	Sel	Prec	Rec	Sel	Prec	Rec	Sel
Top Left	0.69	0.19	7.0	0.32	0.11	9.0	0.29	0.05	4.5
Top Right	0.27	0.11	10.4	0.28	0.20	18.5	0.26	0.09	8.6
Bottom Left	0.33	0.35	27.1	0.27	0.26	24.1	0.26	0.35	34.1
Bottom Right	0.32	0.73	55.6	0.27	0.53	48.3	0.25	0.53	52.0
Invalid			0.01			0.03			0.81

E.2 Light Priors

Within the Light Priors task, we again see preferences. GPT-4o, will routinely prefer a specific quadrant. For example, in Left and Right it selects the top-right cell over 50% of the time. On the other hand, Claude-Sonnet exhibits a strong bias towards selecting the bottom left cell in the Left, Right, and Top variants. Similarly, Llama90B seems to prefer the bottom right quadrant in all task variants. The smaller models all seem to lean towards selecting the Bottom Right quadrant.

Table 6: Model classification performance and predicted proportions on the **Light Priors Task** for GPT-4o, Claude-Sonnet, Llama 90B. Direction corresponds to the direction the target appears to be lit from. “Sel” indicates the percentage of model predictions assigned to each label.

(a) GPT-4o

Label	Bottom			Prec	Left			Prec	Right			Prec	Top	
	Prec	Rec	Sel		Rec	Sel	Prec		Rec	Sel	Rec		Sel	
Top Left	0.82	0.55	17.3	0.46	0.09	4.8	0.71	0.14	5.2	0.78	0.25	8.1		
Top Right	0.64	0.86	33.2	0.45	0.38	20.7	0.43	0.37	21.0	0.54	0.63	29.0		
Bottom Left	0.78	0.77	24.6	0.45	0.35	19.6	0.55	0.46	20.8	0.62	0.58	23.6		
Bottom Right	0.74	0.74	24.8	0.32	0.71	54.7	0.35	0.76	53.0	0.46	0.73	39.3		
Invalid			0.13			0.11			0.06			0.04		

(b) Claude-Sonnet

Label	Bottom			Prec	Left			Prec	Right			Prec	Top	
	Prec	Rec	Sel		Rec	Sel	Prec		Rec	Sel	Rec		Sel	
Top Left	0.67	0.25	9.6	0.46	0.11	6.2	0.51	0.12	6.2	0.54	0.16	7.5		
Top Right	0.47	0.34	17.9	0.35	0.20	13.9	0.34	0.19	13.9	0.36	0.23	15.6		
Bottom Left	0.33	0.80	60.8	0.28	0.74	67.2	0.27	0.75	68.4	0.28	0.76	67.5		
Bottom Right	0.69	0.32	11.5	0.28	0.14	12.8	0.28	0.13	11.5	0.45	0.17	9.3		
Invalid			0.05			0.00			0.01			0.01		

(c) LLaMA-90B

Label	Bottom			Prec	Left			Prec	Right			Prec	Top	
	Prec	Rec	Sel		Rec	Sel	Prec		Rec	Sel	Rec		Sel	
Top Left	0.59	0.70	30.6	0.61	0.47	19.5	0.56	0.33	14.9	0.61	0.73	30.7		
Top Right	0.65	0.20	7.4	0.46	0.21	11.4	0.39	0.19	12.4	0.71	0.19	6.6		
Bottom Left	0.49	0.41	21.2	0.41	0.47	28.8	0.36	0.40	27.6	0.49	0.44	22.5		
Bottom Right	0.49	0.70	35.4	0.41	0.62	36.9	0.36	0.61	41.9	0.48	0.69	35.4		
Invalid			5.43			3.36			3.24			4.88		

Table 7: Classification performance and predicted proportions on the Light Priors Task for GPT-4-Turbo, Claude-Haiku, and Llama 11B. “Sel” indicates the percentage of predictions assigned to each cell.

(a) GPT-4 Turbo

Label	Bottom			Left			Right			Top		
	Prec	Rec	Sel	Prec	Rec	Sel	Prec	Rec	Sel	Prec	Rec	Sel
Top Left	0.35	0.34	25.1	0.28	0.42	38.1	0.28	0.29	26.5	0.26	0.32	31.6
Top Right	0.42	0.05	2.7	0.42	0.01	0.6	0.22	0.01	1.3	0.35	0.01	0.9
Bottom Left	0.97	0.01	0.4	0.00	0.00	0.0	0.25	0.00	0.0	0.00	0.00	0.0
Bottom Right	0.28	0.80	71.9	0.26	0.63	61.3	0.25	0.72	72.2	0.25	0.69	67.4
Invalid			0.00			0.00			0.00			0.00

(b) Claude-Haiku

Label	Bottom			Left			Right			Top		
	Prec	Rec	Sel	Prec	Rec	Sel	Prec	Rec	Sel	Prec	Rec	Sel
Top Left	0.70	0.01	0.3	0.33	0.00	0.0	1.00	0.00	0.0	0.75	0.00	0.1
Top Right	0.43	0.03	1.5	0.42	0.03	1.8	0.41	0.03	1.7	0.42	0.03	1.6
Bottom Left	0.68	0.07	2.7	0.60	0.03	1.3	0.61	0.03	1.2	0.61	0.04	1.6
Bottom Right	0.24	0.88	88.5	0.25	0.96	94.0	0.25	0.98	95.1	0.25	0.98	94.9
Invalid			7.01			2.90			2.03			1.78

(c) LLaMA-11B

Label	Bottom			Left			Right			Top		
	Prec	Rec	Sel	Prec	Rec	Sel	Prec	Rec	Sel	Prec	Rec	Sel
Top Left	0.68	0.09	3.4	0.36	0.06	4.3	0.36	0.07	4.8	0.45	0.07	3.8
Top Right	0.17	0.04	5.1	0.23	0.10	10.7	0.22	0.10	11.0	0.17	0.06	8.5
Bottom Left	0.29	0.36	30.9	0.26	0.37	35.5	0.25	0.34	34.2	0.25	0.35	34.4
Bottom Right	0.30	0.74	60.2	0.27	0.53	49.3	0.27	0.54	49.9	0.26	0.57	53.0
Invalid			0.29			0.17			0.19			0.28

E.3 Circle Sizes

Finally, in the Circle Sizes task, we again see spatial biases from models. Claude-sonnet heavily prefers the bottom left across all size variations. Meanwhile Llama 90B prefers the top-left. For both of these models the strength of preference increases with task difficulty, indicating a sort of “uncertainty response” with the preference. On the other hand GPT-4o eventually heavily prefers the bottom-right, but this is only present in the hardest Small variant. Both GPT-4-Turbo and Claude-Haiku heavily favour the bottom right quadrant, while Llama 11B is split between the bottom right and bottom left.

Table 8: Model classification performance and predicted proportions on the **Circle Sizes Task** for GPT-4o, Claude-Sonnet, and Llama 90B. “Sel” indicates the percentage of model predictions assigned to each label.

(a) GPT-4o

Label	Large			Medium			Small		
	Prec	Rec	Sel	Prec	Rec	Sel	Prec	Rec	Sel
Top Left	0.93	0.74	20.0	0.92	0.51	13.8	0.73	0.15	5.2
Top Right	0.72	0.97	33.3	0.68	0.73	26.8	0.58	0.20	8.6
Bottom Left	0.90	0.85	23.5	0.75	0.82	27.7	0.46	0.58	31.4
Bottom Right	0.91	0.76	21.2	0.69	0.83	29.6	0.37	0.76	51.9
Invalid			2.04			2.14			2.78

(b) Claude-Sonnet

Label	Large			Medium			Small		
	Prec	Rec	Sel	Prec	Rec	Sel	Prec	Rec	Sel
Top Left	0.81	0.27	8.3	0.48	0.29	15.1	0.33	0.28	21.2
Top Right	0.57	0.67	28.9	0.50	0.27	13.4	0.36	0.13	9.0
Bottom Left	0.50	0.93	46.8	0.34	0.79	59.0	0.27	0.70	63.4
Bottom Right	0.84	0.53	15.9	0.68	0.34	12.4	0.42	0.10	6.3
Invalid			0.03			0.04			0.00

(c) LLaMA 90B

Label	Large			Medium			Small		
	Prec	Rec	Sel	Prec	Rec	Sel	Prec	Rec	Sel
Top Left	0.51	0.75	36.6	0.35	0.78	56.4	0.28	0.75	66.3
Top Right	0.66	0.12	4.6	0.54	0.14	6.3	0.35	0.08	5.7
Bottom Left	0.35	0.42	30.0	0.23	0.09	9.7	0.28	0.07	6.4
Bottom Right	0.52	0.56	27.4	0.33	0.35	26.4	0.28	0.22	20.4
Invalid			1.35			1.21			1.22

E.4 Finetuning

In Table 10 we present the preference results within the Shape Conjunctive variatoon for GPT-4o after various levels of finetuning, corresponding to the fine-tuned models described in Section 4 and Appendix H. Here we see that that increased levels of finetuning can reduce the extent of spatial bias inherent in the model. At larger levels (n=100, n=1000) the cell preferences have almost completely disappeared.

F Correlation analysis

A series of Pearson’s correlations were conducted to analyse whether model performance was associated with increasing distractor numbers within task conditions. A pronounced negative correlation suggests the target was increasingly harder to find at higher set sizes, and is indicative of serial search in human participants. A lack of a correlation suggests performance was flat across set sizes. A combination of high performance coupled with set-size independence is indicative of a pop-out effect. The results of this analysis are displayed in Tables 11, 12, and 13.

G Experiment Replication and Computing Resources

All of the experiments in our paper are designed to be replicable and upon publication will be accompanied with a code repository ⁶ which contains detailed guidance on which scripts to run and with what arguments in the README file.

⁶<https://github.com/JohnBurden/ISpyWithMyModelsEye>

Table 9: Classification performance and predicted proportions on the Circle Sizes Task for GPT-4-turbo, Claude-Haiku, and LLaMA 11B. “Sel” indicates the percentage of predictions assigned to each cell.

(a) GPT-4-turbo

Label	Large			Medium			Small		
	Prec	Rec	Sel	Prec	Rec	Sel	Prec	Rec	Sel
Top Left	0.70	0.25	8.9	0.44	0.16	9.0	0.35	0.12	8.6
Top Right	0.43	0.32	18.1	0.37	0.18	11.7	0.35	0.16	11.2
Bottom Left	0.52	0.33	15.9	0.31	0.18	14.7	0.33	0.21	15.5
Bottom Right	0.36	0.81	57.0	0.28	0.74	64.7	0.27	0.70	64.6
Invalid			0.08			0.02			0.01

(b) Claude-Haiku

Label	Large			Medium			Small		
	Prec	Rec	Sel	Prec	Rec	Sel	Prec	Rec	Sel
Top Left	0.98	0.02	0.6	0.93	0.01	0.3	0.81	0.01	0.3
Top Right	0.41	0.01	0.8	0.30	0.00	0.3	0.54	0.01	0.3
Bottom Left	0.73	0.38	13.1	0.57	0.05	2.1	0.47	0.03	1.3
Bottom Right	0.30	0.87	72.3	0.25	0.91	89.3	0.26	0.95	93.6
Invalid			13.18			8.09			4.49

(c) LLaMA 11B

Label	Large			Medium			Small		
	Prec	Rec	Sel	Prec	Rec	Sel	Prec	Rec	Sel
Top Left	0.35	0.15	10.8	0.28	0.15	13.7	0.29	0.15	13.0
Top Right	0.24	0.08	8.7	0.26	0.10	9.4	0.24	0.09	9.7
Bottom Left	0.26	0.42	40.9	0.26	0.40	40.0	0.25	0.40	40.5
Bottom Right	0.26	0.41	39.4	0.25	0.37	36.9	0.25	0.37	36.7
Invalid			0.15			0.06			0.12

Table 10: GPT-4o’s classification performance and predicted proportions across levels of finetuning set-sizes. (n). “Sel” indicates the percentage of predictions assigned to each label.

Label	$n = 0$			$n = 10$			$n = 100$			$n = 1000$		
	Prec	Rec	Sel	Prec	Rec	Sel	Prec	Rec	Sel	Prec	Rec	Sel
Top Left	0.91	0.30	8.1	0.84	0.53	15.7	0.84	0.77	22.7	0.78	0.89	28.4
Top Right	0.55	0.74	33.8	0.65	0.74	28.2	0.73	0.86	29.4	0.89	0.77	21.8
Bottom Left	0.72	0.53	18.8	0.64	0.77	30.2	0.81	0.83	25.9	0.84	0.85	25.7
Bottom Right	0.51	0.72	35.2	0.61	0.63	25.6	0.81	0.72	22.0	0.85	0.82	24.1
Invalid			4.07			0.32			0.00			0.00

The code contains everything needed to generate the exact images we used, including any random seeds we set. The images were generated with seed 42.

The code contains scripts to generate and submit batches to either Anthropic or OpenAI, or to submit models to a local SLURM cluster (though users will need to provide their own appropriately set up SLURM scripts. Finally, the code also contains our scripts for generating figures used in the paper. Upon publication we also intend to release our instance-level responses from each model to each question.

The biggest obstacle to replication is cost or access to compute. The experiments using the GPT and Claude Models rely on paid API access and in total cost multiple hundreds of dollars to run all of these experiments. Nevertheless,

Table 11: Correlation (Pearson’s r) between number of distractors and accuracy across AI models and conditions in the Circle Sizes task. The reported p -values are adjusted using the Bonferroni correction for multiple comparisons.

Model	Small		Medium		Large	
	r	p	r	p	r	p
claude-haiku	-0.039	0.002	-0.047	< .001	-0.101	< .001
claude-sonnet	-0.111	< .001	-0.166	< .001	-0.136	< .001
gpt-4-turbo	-0.100	< .001	-0.126	< .001	-0.159	< .001
gpt-4o	-0.177	< .001	-0.102	< .001	-0.028	0.082
llama11B	-0.018	1.000	-0.016	1.000	-0.009	1.000
llama90B	-0.029	0.057	0.032	0.021	0.081	< .001

Table 12: Correlation (Pearson’s r) between number of distractors and accuracy across AI models and conditions in the Two Among Five task. The reported p -values are adjusted using the Bonferroni correction for multiple comparisons.

Model	Disjunctive		Shape Conjunctive		Shape-Colour Conjunctive	
	r	p	r	p	r	p
claude-haiku	-0.156	< .001	-0.124	< .001	-0.048	< .001
claude-sonnet	-0.065	< .001	-0.159	< .001	-0.219	< .001
gpt-4-turbo	-0.135	< .001	-0.215	< .001	-0.148	< .001
gpt-4o	0.017	0.249	-0.267	< .001	-0.244	< .001
llama11B	0.015	0.700	-0.017	0.265	-0.014	0.885
llama90B	0.010	1.000	-0.100	< .001	-0.100	< .001

this reduces compute burden on the user. For both providers the API batching option was used to reduce cost, but this makes it difficult to anticipate the total compute used or time required.

To run the Llama models we used an internal HPC cluster with exclusive access to nodes consisting of 4 Nvidia A100s. Each Llama experiment took around 16-18 hours, but was split into two batches across two nodes. In total, for Llama 90B, we used approximately 450 hours of compute on these A100s.

H Finetuning Details

Our finetuning was conducted using OpenAI’s supervised finetuning API⁷ for GPT-4o. Models were trained on images from the Shape Conjunctive 2 Among 5s task generated with seed 1745313698. The evaluation seeds were: 1745332147 for Shape Conjunctive 2 Among 5, 1745566567 for Shape Conjunctive T Among Ls, 1746005099 for Disjunctive T Among Ls, and 1746104336 for Shape-Colour Conjunctive 2 Among 5.

The Ts Among Ls task is functionally the same as the 2 Among 5 task except the targets are representations of Ts and the distractors Ls. An example instance is given in Figure 17. While similar, the specific targets and distractors are visually distinct from the 2s and 5s, yet the same broad skill is required (identifying a target based on spatial features alone, not colours).

Figure 18 shows plots for all out-of-distribution evaluations we performed on the fine-tuned models. We see mild, but significant, improved performance on the Shape Conjunctive task with T among Ls.

I Human Baselines

I.1 Participants

Human participants for the three visual search tasks (Circle Sizes, Two Among Five and Light Priors) were recruited online using *Prolific* (www.prolific.co). Following ethics approval from our institution’s Research Ethics Committee. We recruited 30 participants for each task (Total N = 90, Age $M = 35$, 45 female, 45 male). Participants were pre-screened to ensure they were in the age range 18-60, were fluent in reading English, and self-reported normal or corrected-to-normal

⁷<https://platform.openai.com/docs/guides/fine-tuning>

Table 13: Correlation (Pearson’s r) between number of distractors and accuracy across AI models and conditions in the Light Priors task. The reported p -values are adjusted using the Bonferroni correction for multiple comparisons.

Model	Left		Bottom		Right		Top	
	r	p	r	p	r	p	r	p
claude-haiku	-0.063	< .001	-0.112	< .001	-0.067	< .001	-0.056	< .001
claude-sonnet	-0.109	< .001	-0.102	< .001	-0.138	< .001	-0.139	< .001
gpt-4-turbo	-0.024	0.415	-0.064	< .001	-0.022	0.745	-0.029	0.087
gpt-4o	0.072	< .001	0.200	< .001	-0.053	< .001	-0.120	< .001
llama11B	-0.029	0.088	-0.002	1.000	-0.032	0.028	-0.017	1.000
llama90B	0.117	< .001	0.084	< .001	0.104	< .001	0.038	0.003



Figure 17: An example of the T Among Ls task.

colour vision. To maintain data quality, we replaced participants whose mean accuracy fell below chance level (25%, $N = 0$). Participants were compensated at the standard rate for their time and participation (£1.25, approximately £7.50/hour).

I.2 Stimuli and procedure

Stimuli for the human baseline experiments were drawn from subsets of the AI test-sets. To construct the human stimulus sample, we used a stratified random sampling procedure within each experimental condition. Specifically, four stimuli were randomly selected from different distractor size ranges (or bins; see Table 14). Within each bin, target locations were evenly distributed, with each of the four Cells represented once. Colour combinations in the Two Among Five and Circle Size tasks were balanced within conditions. Prior to sampling, we excluded all stimuli with targets

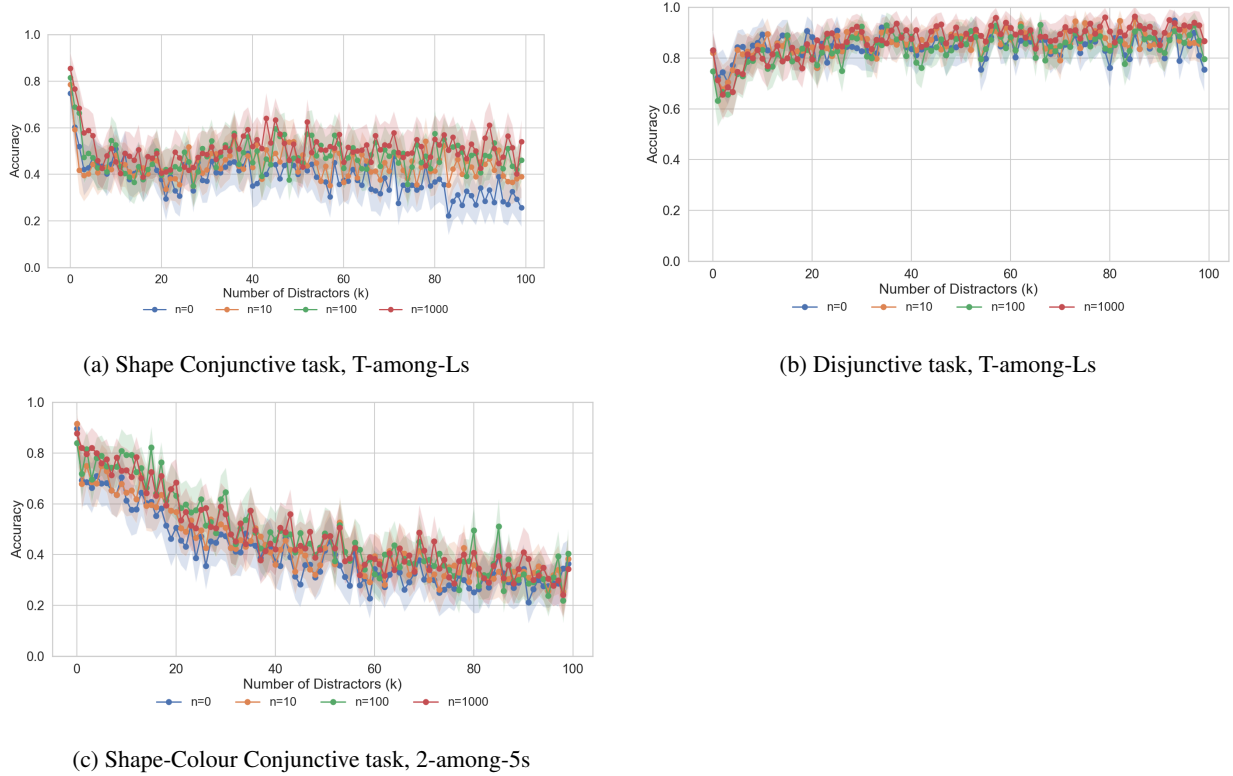


Figure 18: Fine-tuned GPT-4o evaluation

located within the coordinate range of 170–230 on either axis to prevent targets from appearing along the borders between Cells.

Table 14: Distractor bin sizes

Circle Sizes	Two Among Five	Light Priors
1–4	1–4	2–5
5–8	5–8	6–9
9–12	9–16	10–13
13–16	17–32	14–17
17–20	33–64	
21–24	65–99	
25–28		
29–32		
33–36		
37–40		
41–44		
45–49		

I.2.1 Circle Sizes

In the Circle Sizes task, we implemented a 3 (Condition: Small, Medium, Large) \times 12 (Distractor Number: twelve bins) factorial design, with four trials per bin, resulting in 144 trials overall.

The experiment was conducted online using *Gorilla* (<https://gorilla.sc/>). After obtaining informed consent and checking their use of a QWERTY keyboard, participants were informed they would need to locate the largest circle amongst distractors, responding with the corresponding Cell using the keys Q (top-left), P (top-right), A (bottom-left) or L (bottom-right). Participants were provided with two examples followed by eight practice trials with feedback to

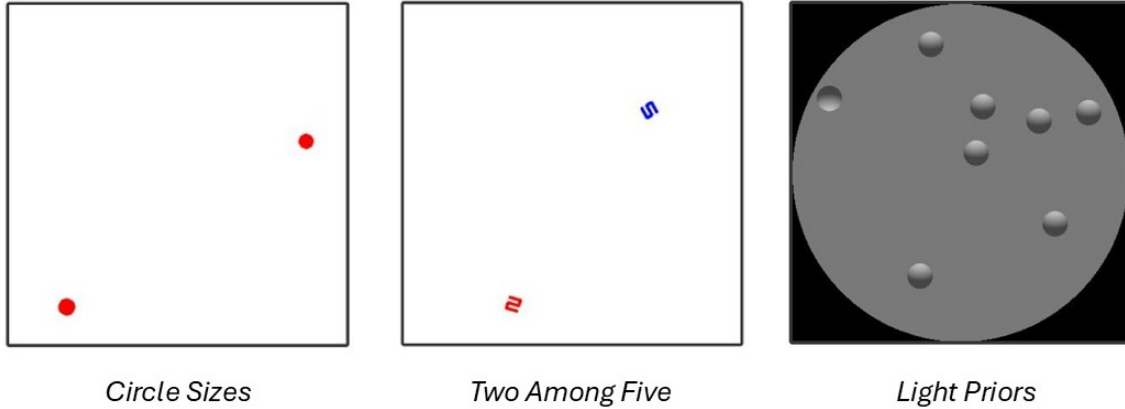


Figure 19: Screenshots from experimental trials presented to online participants in Two Among Five (Left; "Find the red 2"), Light Priors (Middle; "Find the odd one out") and Circle Sizes tasks (Right; "Find the largest circle").

familiarise with the response keys. Participants were also informed that when in doubt as to which cell the target was in, they should respond with the Cell that they believe the target was “most in”, and if the image disappeared before they located the target, they should respond with their best guess.

Experimental trials were preceded with a central fixation cross (for 500ms). The 400×400 pixel image stimulus then appeared centrally at full resolution, accompanied by the prompt “Find the largest circle” (see Figure 19). The image stimulus remained on screen for 1500 milliseconds before being replaced by a white image mask.

I.2.2 Two Among Five task

For the Two Among Five task, we employed a 3 (Condition: Disjunctive, Shape Conjunctive, Shape-Colour Conjunctive) \times 2 (Version: 2 Among 5, 5 Among 2) \times 6 (Distractor Number: six bins) factorial design, again with four trials per bin, resulting in a total of 144 trials. The experimental procedure was the same as in the Circle Sizes task, except the prompt said “Find the *colour number*” — with *colour* and *number* replaced with the correct target features (e.g., "Find the red 2"), and the stimulus appeared on screen for 3000ms to maintain similar difficulty levels on this task which included trials with a higher number of distractors (e.g., 99).

I.2.3 Light Priors

Finally, in the Light Priors task, we used a 2 (Condition: Vertical Gradient, Horizontal Gradient) \times 2 (Version: Original [Top-lit, Left-lit], Reversed [Bottom-lit, Right-lit]) \times 4 (Distractor Number: Four bins) factorial design, with twelve trials per bin, yielding 192 trials in total. The experiment procedure was the same as the Two Among Five task, except participants were told the image would contain spheres lit from different directions, and were instructed to "Find the odd one out" (e.g., a bottom-lit sphere amongst top-lit spheres; see Figure 19). The Light Priors task uses fewer distractors (here 2–17) to prevent the spheres becoming tightly clustered and the target easily identified through contrast with proximal distractors (Adams, 2007). We also did not include single-distractor trials as at least two distractors are required to identify an "odd one out". Given these reduced set sizes, we decreased the image presentation time to 1500 milliseconds to maintain difficulty levels.

I.3 Results

I.3.1 Circle Sizes task

Table 15 displays the results for human performance in the Circle Sizes task, which we analysed using a 3 (Condition: Small, Medium, Large) \times 12 (Distractor Number: twelve bins) \times 4 (Cell: top-left, top-right, bottom-left, bottom-right) repeated measures ANOVA. Performance in the Large target condition was close to ceiling ($M = 96\%$), and accuracy was higher than in the Medium condition ($M = 88\%$, $t = 8.42$, $p < .001$), and accuracy in both of these conditions was higher than the Small condition ($M = 59\%$, $ts > 18.9$, $ps < .001$). Overall performance declined with increasing Distractor Number, but a Distractor Number \times Condition interaction indicates that this effect was not uniform across all size conditions. For Large targets, all comparisons between distractor bin pairs were non-significant ($ts < 2.8$, $ps >$

.06), indicating a clear pop-out effect. In the Medium condition, only the difference between bins 13–16 and 45–49 were significant ($t = 4.76$, $ps = .004$, all other $ts < 3.5$, $ps > .05$), suggesting a large degree of set size independence. Performance declined steadily with set size in the Small condition (e.g., bin 1–4 vs 45–49: $t = 5.11$, $p < .001$).

We also found a main effect of Cell, and a marginal Cell \times Condition interaction. While participants showed similarly high accuracy across Cells in the Large condition (all $Ms > 95\%$), differences were found in the Small and Medium condition. Overall, accuracy was lowest for the bottom-right cell ($M = 78\%$), perhaps reflecting a serial search strategy ending in the bottom-right quadrant of the screen.

Table 15: ANOVA results for human performance in the Circle Sizes task.

Effect	DFn	DFd	F	p	η_p^2
Condition	1.27	36.85	246.391	<.001	0.895
Cell	3.00	87.00	4.593	0.005	0.137
Distractor Number	11.00	319.00	7.811	<.001	0.212
Condition \times Cell	3.87	112.33	2.336	0.062	0.075
Condition \times Distractor Number	10.86	315.00	2.938	0.001	0.092
Cell \times Distractor Number	33.00	957.00	2.625	<.001	0.083
Condition \times Cell \times Distractor Number	66.00	1914.00	2.114	<.001	0.068

I.3.2 Two Among Five task

To analyse the performance of human participants in the Two Among Five task, we conducted a 3 (Condition: Disjunctive, Shape Conjunctive, Shape-Colour Conjunctive) \times 2 (Version: 2 Among 5, 5 Among 2) \times 6 (Distractor Number: six bins) \times 4 (Cell: top-left, top-right, bottom-left, bottom-right) repeated measures Analysis of Variance (ANOVA), summarised in Table 16.

Table 16: ANOVA results for human performance in the Two Among Five task.

Effect	DFn	DFd	F	p	η_p^2
Condition	2.00	58.00	115.831	<.001	0.800
Version	1.00	29.00	0.549	0.465	0.019
Cell	3.00	87.00	13.318	<.001	0.315
Distractor Number	5.00	145.00	50.839	<.001	0.637
Condition \times Version	2.00	58.00	0.060	0.942	0.002
Condition \times Cell	4.08	118.43	5.866	<.001	0.168
Version \times Cell	3.00	87.00	0.567	0.638	0.019
Condition \times Distractor Number	10.00	290.00	17.486	<.001	0.376
Version \times Distractor Number	5.00	145.00	1.026	0.405	0.034
Cell \times Distractor Number	15.00	435.00	2.110	0.009	0.068
Condition \times Version \times Cell	4.03	116.89	2.398	0.054	0.076
Condition \times Version \times Distractor Number	6.40	185.55	1.435	0.199	0.047
Condition \times Cell \times Distractor Number	30.00	870.00	2.524	<.001	0.080
Version \times Cell \times Distractor Number	15.00	435.00	0.935	0.525	0.031
Condition \times Version \times Cell \times Distractor Number	30.00	870.00	0.709	0.876	0.024

Participants’ performance in the Disjunctive condition was at ceiling ($M = 98\%$) and overall higher than in the Shape Conjunctive ($M = 64\%$, $t = 26.14$, $p < .001$), and Shape-Colour Conjunctive conditions ($M = 69\%$, $t = 22.88$, $p < .001$)⁸. Shape-Colour Conjunctive performance was also higher than Shape Conjunctive ($t = 3.22$, $p = .004$). Participant performance overall decreased with Distractor Number (see Figure 3), but unlike other conditions, differences between Distractor Number bins within the Disjunctive condition were all non-significant (all $ts < 2.9$, $ps > .06$), suggesting pop-out performance in that condition. In the Shape Conjunctive (e.g., bin 1–4 vs 65–99: $t = 12.96$, $p < .001$) and Shape-Colour Conjunctive (e.g., bin 1–4 vs 65–99: $t = 8.44$, $p < .001$) conditions, accuracy declined across set size, indicating serial search.

Participant performance was similar across Versions, but like the previous experiment, performance differed depending on which Cell the target number was located. This effect interacted with Condition, and post-hoc tests indicated

⁸All post-hoc p-values are adjusted for multiple comparisons using the Bonferroni correction

performance between Cells were not significantly different in the Disjunctive or Shape Conjunctive conditions (all $t_s < 2.3$, $p_s > .15$). In the Conjunctive condition, participants showed reduced accuracy in the bottom-right cell ($M = 54\%$) relative to the others (all $t_s > 4.9$, $p_s < .001$), likely reflecting a serial search strategy ending in the bottom-right quadrant of the screen.

I.3.3 Light Priors task

For the Light Priors task, we conducted a 2 (Condition: Vertical Gradient, Horizontal Gradient) \times 2 (Version: Original, Reversed) \times 4 (Distractor Number: Four bins) \times 4 (Cell: top-left, top-right, bottom-left, bottom-right) repeated measures ANOVA, the results of which are displayed in Table 17. An effect of Condition showed humans performed better in the vertical ($M = 86\%$) relative to the horizontal gradient condition overall ($M = 65\%$), though performance in both conditions was flat across across set sizes. We also found an effect of Version, and a marginal Condition \times Version interaction. Post-hoc tests indicate that participants were slightly better at detecting right-lit ($M = 67\%$) compared to left-lit ($M = 63\%$) lit spheres ($t = 2.30$, $p = 0.021$), but substantially better at detecting bottom-lit ($M = 91\%$) compared to top-lit ($M = 81\%$) spheres ($t = 8.23$, $p = <.001$). Improved performance for vertical gradients, and for the novel ‘bottom-lit’ variant in particular, is consistent with findings from classic studies (Enns and Rensink, 1990).

Table 17: ANOVA results for human performance in the Light Priors task.

Effect	DF_n	DF_d	F	p	η_p^2
Condition	1.00	29.00	91.528	<.001	0.759
Inversion	1.00	29.00	18.007	<.001	0.383
Cell	3.00	87.00	1.578	0.200	0.052
Distractor Number	3.00	87.00	1.109	0.350	0.037
Condition \times Inversion	1.00	29.00	3.005	0.094	0.094
Condition \times Cell	3.00	87.00	2.293	0.084	0.073
Inversion \times Cell	3.00	87.00	0.789	0.503	0.027
Condition \times Distractor Number	3.00	87.00	0.742	0.530	0.025
Inversion \times Distractor Number	3.00	87.00	2.245	0.089	0.072
Cell \times Distractor Number	9.00	261.00	2.401	0.012	0.076
Condition \times Inversion \times Cell	3.00	87.00	2.849	0.042	0.089
Condition \times Inversion \times Distractor Number	3.00	87.00	2.466	0.068	0.078
Condition \times Cell \times Distractor Number	9.00	261.00	3.336	0.001	0.103
Inversion \times Cell \times Distractor Number	9.00	261.00	1.376	0.199	0.045
Condition \times Inversion \times Cell \times Distractor Number	9.00	261.00	1.825	0.064	0.059

J Prompting Details

In Tables 18, 19, and 20 we detail the prompts that were used throughout our experiments with the MLLMs.

We aimed to keep these as similar to each other as feasible, but were forced to adapt a few prompts to either provide sufficient information to the model, or to force models to respond. For instance, the Shape-Colour Conjointive search in the Two Among Five task requires additional information to solve compared to the other variations (both the colour and shape need to be provided instead of just shape). On the other hand, when requesting some models for coordinates, some models (Claude Sonnet and Llama90B in particular) would rarely provide coordinates unless you offered them the chance to explain their uncertainty.

Table 18: Prompts used for the 2Among5 tasks. Bolded terms indicate that the prompt includes the appropriate target, distractor, or colour for the image instance.

Experiment	Prompt
2Among5 Shape Conjointive Search (Cells)	The image is divided into a 2x2 grid. Each element of the grid is referred to as a cell. In the presented image there are a number of objects. Almost all of the objects are the number distractor written as a numeral. There is a single target in the image, similarly represented by a numeral. In which cell is the target in? In the case where the target overlaps multiple cells, please provide the cell where the centre of the target is located. Please only respond with 'Cell (i,j)' where (i,j) corresponds to the ith row and jth column of the grid. The top left cell is Cell (1,1). Do not reply with anything else.
2Among5 Shape-Colour Conjointive (Cells)	The image is divided into a 2x2 grid. Each element of the grid is referred to as a cell. In the presented image there are a number of objects. There are '2's and '5's written as numerals. In which cell is the colour 'shape'? In the case where the colour 'target' overlaps multiple cells, please provide the cell where the centre of the shape is located. Please only respond with 'Cell (i,j)' where (i,j) corresponds to the ith row and jth column of the grid. The top left cell is Cell (1,1). If you are uncertain you may optionally add a note explaining that but please start your response with 'Cell (i,j)'.
2Among5 Shape Conjointive Search (Coordinates)	The presented image is 400x400 pixels large, and the origin (0,0) is in the top left of the image. In the presented image there are a number of objects. Almost all of the objects are the number distractor written as a numeral. There is a single target in the image, similarly represented by a numeral. What are the coordinates of the centre of the target ? Please give your best estimate. If you are uncertain please guess but optionally add a description to note this. However, for ease of processing please begin your response with a set of coordinates using round brackets.
2Among5 Shape-Colour Conjointive Search (Coordinates)	The presented image is 400x400 pixels large, and the origin (0,0) is in the top left of the image. In the presented image there are a number of objects. There are '2's and '5's written as numerals. What are the coordinates of the colour 'target' ? Please give your best estimate. If you are uncertain please guess but optionally add a description to note this. However, for ease of processing please begin your response with a set of coordinates using round brackets.

Table 19: Prompts used for the Light Priors tasks. Bolded terms indicate that the prompt includes the appropriate shading directions for the image instance.

Experiment	Prompt
Light Priors (Cells)	The image is divided into a 2x2 grid. Each element of the grid is referred to as a cell. In the presented image there are a number of spheres lit from different directions. Almost all of the spheres are lit from the same direction, but one sphere is lit from the opposite direction. In which cell is this oppositely lit sphere? In the case where the sphere overlaps multiple cells, please provide the cell where the centre of the sphere lit from the opposite direction is located. Please only respond with 'Cell (i,j)' where (i,j) corresponds to the ith row and jth column of the grid. The top left cell is Cell (1,1). If you are uncertain please guess but optionally add a description to note this. However, for ease of processing please begin your response with 'Cell (i,j)'.
Light Priors (Coordinates)	The presented image is 400x400 pixels large, and the origin (0,0) is in the top left of the image. In the presented image there are a number of spheres lit from different directions. Almost all of the spheres are lit from the same direction, but one sphere is lit from the opposite direction. What are the coordinates of the centre of the oppositely lit sphere? If you are uncertain please guess but optionally add a description to note this. However, for ease of processing please begin your response with a set of coordinates using round brackets."

Table 20: Prompts used for the Circle Sizes tasks.

Experiment	Prompt
Circle Sizes (Cells)	The image is divided into a 2x2 grid. Each element of the grid is referred to as a cell. In the presented image there are a number of circles. One of the circles is larger than the rest. In which cell is the larger circle? In the case where the larger circle overlaps multiple cells, please provide the cell where the centre of the larger circle is located. Please only respond with 'Cell (i,j)' where (i,j) corresponds to the ith row and jth column of the grid. The top left cell is Cell (1,1). If you are uncertain you may optionally add a note explaining that but please start your response with 'Cell (i,j)'.
Circle Sizes (Coordinates)	The presented image is 400x400 pixels large, and the origin (0,0) is in the top left of the image. In the presented image there are a number of circles. One of the circles is larger than the others. What are the coordinates of the larger circle? Please give your best estimate. If you are uncertain please guess but optionally add a description to note this. However, for ease of processing please begin your response with a set of coordinates using round brackets.

K Mechanistic Interpretability

K.1 Experimental Details

Tasks and stimuli. We evaluate on the 3 main tasks (Circle Sizes, 2Among5, and Light Priors, breaking down into the constituent datasets (e.g., CircleSizes Small, Medium, and Large are evaluated seperately).

For each experiment we sample 300 images uniformly across the number of distractors (field size n), and store per-image metadata (e.g., num_distractors, size, quadrant).

Model and activations. Unless stated, we use Llama-3.2-90B-Vision-Instruct (abbrev. llama90B). During generation we hook three representative language layers (early, middle, late) and record: residual stream, attention output, MLP output, and layer-norm outputs. We also expose minimal vision encoder residuals and projector I/O. Activations are captured at the last prompt token. This yields per-category dicts keyed by `layer_<idx>` with feature shape $[1, 1, d]$.

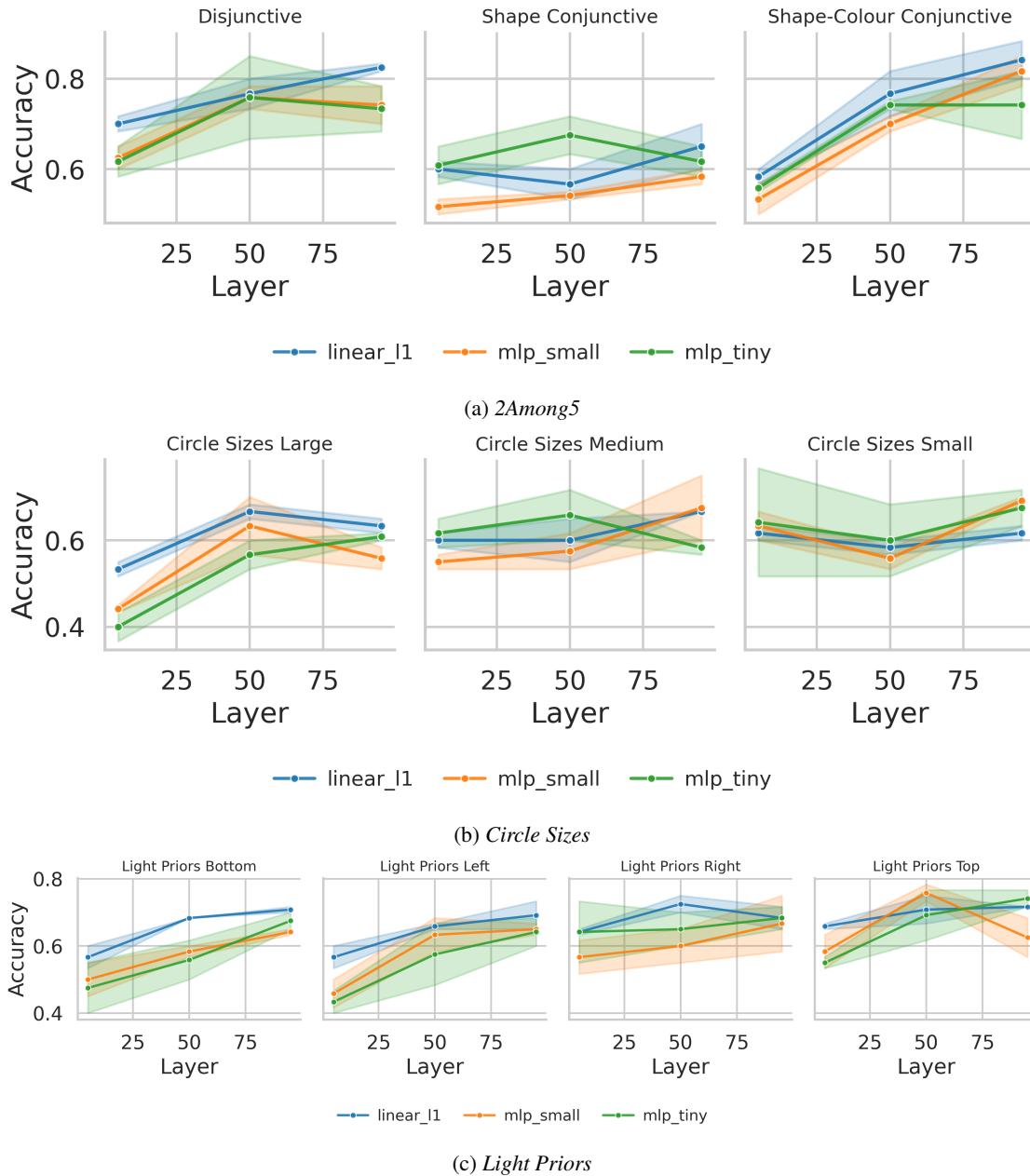
Probes. We train linear and small non-linear readouts. The linear probe is a single-layer logistic model with L1 penalty (trained in PyTorch with BCE-with-logits and Adam). We use an 80/20 stratified split, grid-search $\lambda_{l1} \in \{10^{-3}, 5 \times 10^{-4}, 10^{-4}, 5 \times 10^{-5}, 10^{-5}\}$, batch size 64, and 8 epochs. We also report two MLP probes:

mlp_small (256 hidden units) and mlp_tiny (128→32). Optional stability selection bootstraps estimate feature-selection frequency. We report validation accuracy per (category, layer).

Hardware. Initial activation extraction and probe training were run on 4×A100 (CUDA enabled).

K.2 Experimental Results

We report results from a series of mechanistic probing experiments across tasks designed to test visual search phenomena in LLaMA-90B. Performance is summarized layer by layer, with both linear and nonlinear probes applied to the residual stream. In the *2Among5* task, probe accuracy rises sharply in middle layers, indicating that distinctive-item representations become linearly separable (Figure 20a). For the *Circle Sizes* task, accuracy steadily increases with layer depth, suggesting progressive encoding of size distinctions (Figure 20b). In the *Lit Spheres* task, probes capture light-prior information only in later layers, reflecting delayed emergence of shading-sensitive features (Figure 20c).

Figure 20: Layer-wise probe accuracy across tasks: *2Among5*, *Circle Sizes*, and *Light Priors*.